

RESEARCH ARTICLE SUMMARY

NEUROSCIENCE

Identification of the subventricular tegmental nucleus as brainstem reward center

Krisztián Zichó, Boldizsár Zsolt Balog, Réka Z. Sebestény, János Brunner, Virág Takács, Albert M. Barth, Charlotte Seng, Áron Orosz, Manó Aliczki, Hunor Sebők, Eva Mikics, Csaba Földy, János Szabadics, Gábor Nyíri*

INTRODUCTION: Reward processing in the brain is essential for guiding goal-directed behavior, shaping motivational states, and regulating mood. This process involves evaluating and predicting the affective valence of stimuli (their intrinsic quality as either good or bad), a function supported by an evolutionarily ancient subcortical neural network. Dopamine release from the ventral tegmental area (VTA) plays a central role in decision-making, adaptive behaviors, and facilitating memory formation, by linking rewards to actions that yield positive outcomes. The ventral tegmental area is tightly regulated by the lateral habenula (LHb), a critical hub for assessing and predicting the emotional value of stimuli and mediating responses to negative experiences. The balanced activity of the LHb-

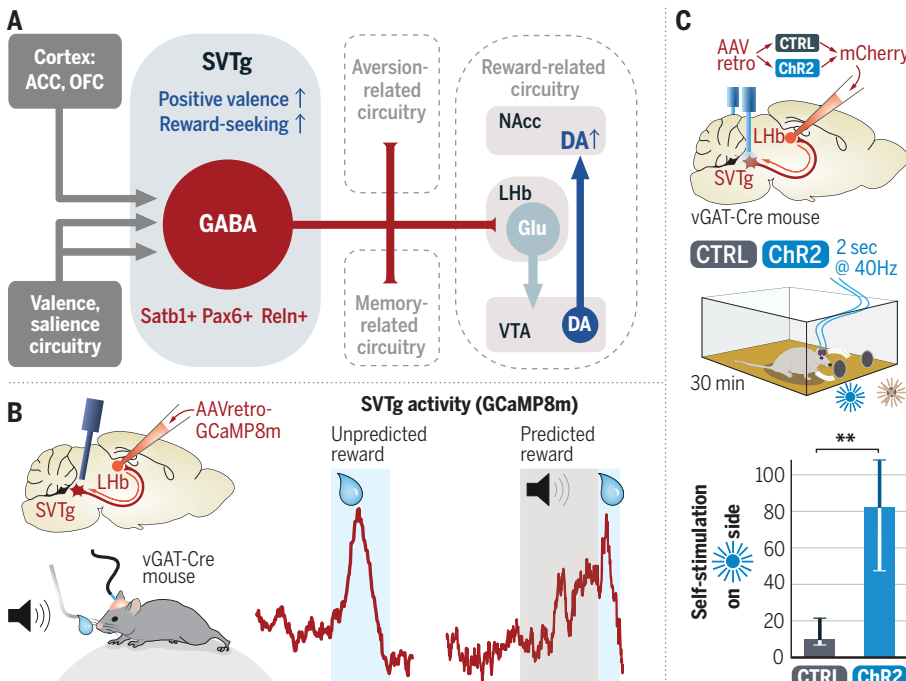
ventral tegmental area axis is therefore crucial for memory formation, prediction, and the maintenance of mental health.

RATIONALE: Negative events strongly activate the LHb, but its overactivation can contribute to anxiety and depression, underscoring the importance of precise regulation. Conversely, inhibiting LHb activity signals positive valence and has shown therapeutic potential in treating depression, as evidenced by the effects of deep brain stimulation and ketamine. Despite decades of research, the primary inhibitory inputs to the LHb remain incompletely understood. In this study, we identified a previously uncharacterized brainstem nucleus beneath the fourth ventricle, which we named the sub-

ventricular tegmental nucleus (SVTg). This nucleus provides abundant inhibitory innervation to the LHb. To investigate the role of the SVTg in reward processing, we employed a multidisciplinary approach, including cell type-specific viral tracing, monosynaptic rabies tracing, single-cell RNA sequencing, *in vivo* and *in vitro* electrophysiology, fiber photometry, and optogenetic behavioral experiments.

RESULTS: We discovered that the SVTg is a γ -aminobutyric acid (GABA)-ergic inhibitory nucleus receiving inputs from regions involved in valence, salience, and memory processing. The SVTg provides the largest purely inhibitory inputs to the LHb and inhibits several other brain regions linked to negative experiences (Fig. A). The SVTg is activated by reward and reward-predicting cues (Fig. B) but not by neutral environmental stimuli, and it can regulate reward location memory. SVTg stimulation induced a positive motivational state, place preference, reduced anxiety, and triggered reward-related dopamine release in the nucleus accumbens, highlighting its role in reward processing. When given the opportunity, mice self-stimulated the SVTg (Fig. C), suggesting its role in reward-seeking behavior. Conversely, SVTg suppression caused place aversion and increased fear. Associational cortices, including the anterior cingulate and other prefrontal cortical regions, target the SVTg. The orbitofrontal cortex (OFC) signals positive valence through the SVTg, whereas serotonergic neurotransmission activates it through distinct mechanisms. Precisely timed SVTg activity prevents excessive fear responses. Our genetic analysis identified selective protein markers for the SVTg, enabling its localization in the brainstem across mice, rats, monkeys, and humans.

CONCLUSION: Our study identifies the SVTg as a GABAergic inhibitory brainstem reward center that integrates inputs from prefrontal cortical and subcortical regions to process affective valence. It controls several brain areas associated with negative emotional states, including the LHb. The SVTg plays a critical role in continuously regulating the brain's valence circuitry, signaling reward and preventing overactivation of aversion circuits during negative events. Given its evolutionary conservation across species, understanding the function and potential dysfunction of the mammalian SVTg may provide valuable insights into emotional and fear-related disorders such as anxiety, depression, and possibly addiction. ■



SVTg, a brainstem reward center. (A) SVTg GABAergic neurons promote positive valence by inhibiting LHb and other aversion-related nuclei. ACC, anterior cingulate cortex; DA, dopamine; Glu, glutamatergic; NAcc, nucleus accumbens. (B) The SVTg of awake mice are activated by unpredicted and predicted reward. AAVretro, retrogradely adeno-associated viruses; vGAT, vesicular GABA transporter. (C) Mice optogenetically self-stimulated their SVTg (with light-sensitive ChR2), compared with control (CTRL) mice. Medians and interquartile ranges.

The list of author affiliations is available in the full article online.

*Corresponding author. Email: nyiri.gabor@koki.hun-ren.hu

Cite this article as K. Zichó et al., *Science* **387**, eadrl2191 (2025). DOI: 10.1126/science.adrl2191

S READ THE FULL ARTICLE AT
<https://doi.org/10.1126/science.adrl2191>

RESEARCH ARTICLE

NEUROSCIENCE

Identification of the subventricular tegmental nucleus as brainstem reward center

Krisztián Zichó^{1,2}, Boldizsár Zsolt Balog^{1,3}, Réka Z. Sebestény¹, János Brunner⁴, Virág Takács¹, Albert M. Barth¹, Charlotte Seng⁵, Áron Orosz^{1,2}, Manó Aliczki⁶, Hunor Sebők¹, Eva Mikics⁶, Csaba Földy⁵, János Szabadics⁴, Gábor Nyíri^{1*}

Rewards are essential for motivation, decision-making, memory, and mental health. We identified the subventricular tegmental nucleus (SVTg) as a brainstem reward center. In mice, reward and its prediction activate the SVTg, and SVTg stimulation leads to place preference, reduced anxiety, and accumbal dopamine release. Mice self-stimulate the SVTg, which can also be activated directly by the neocortex, resulting in effective inhibition of the lateral habenula, a region associated with depression. This mechanism may also explain why SVTg suppression induces aversion and increases fear. The translational relevance of these findings is supported by evidence in the rat, monkey, and human brainstem, establishing SVTg as a key hub for reward processing, emotional valence, and motivation.

Assessing and predicting the affective valence of a stimulus [its quality of being good (appealing) or bad (repulsive)] (1) are complex neuronal processes that involve an evolutionarily ancient subcortical neural network (2–8). These processes are critical because underestimation of negative valence can be fatal whereas its frequent overestimation can, for example, lead to anxiety- and depression-related disorders in humans (9–11).

Valence detection and prediction in the mammalian brain requires the lateral habenula (LHb) (5, 6, 12–14). The LHb integrates value-based, experience-dependent information to regulate motivational and cognitive processes (3, 13, 15–18). Excitatory inputs of LHb induce avoidance, aversion, and aggressive behavior (19–26), whereas its overactivation is found in mouse models of depression and anxiety (27–34) and in major depression disorder in human patients (9–11). Therefore, balancing the activation of LHb is essential.

Inhibition of the LHb can signal positive valence and reward, fine-tune the calculation of “negative reward prediction error” (a hallmark process of the LHb), and is critical for behavioral flexibility and decision-making

(5, 6, 13, 22, 24, 35–37). In a clinical context, deep brain stimulation- or ketamine-induced inactivation of LHb is known to result in complete remission or alleviation of major depression symptoms (9, 27–29, 38, 39). Thus, understanding the inhibitory control of the LHb has important translational implications. Previous studies have suggested that LHb is inhibited primarily by brain areas that send mixed excitatory/inhibitory projections to the LHb, by co-releasing glutamate with the inhibitory gamma-aminobutyric acid (GABA) (21, 22, 24, 40–42). However, despite decades of progress, our understanding of LHb inhibition remains incomplete.

We identify a previously unrecognized inhibitory GABAergic reward-related nucleus in the pontine brainstem, which we named the subventricular tegmental nucleus (SVTg). We described the SVTg as an important pontine reward center that can also effectively balance negative valence processing and among its several targets, and it provides the largest purely inhibitory input to the LHb.

The SVTg, the largest purely inhibitory input nucleus of the LHb

We investigated the GABAergic neuronal inputs of the LHb by injecting a fluorescent protein-expressing, Cre-dependent, retrogradely spreading adeno-associated virus (AAV) into the LHb of vesicular GABA transporter-Cre (vGAT-Cre) mice (Fig. 1A). This revealed a previously unrecognized brain area, the SVTg, under the fourth ventricle in the brainstem pontine central gray (PCG) (Fig. 1B).

After quantifying all retrogradely labeled neurons in the entire mouse brain, we found that about 15% of the GABAergic input neurons projecting to the LHb originated from the SVTg (fig. S1, A and B, and table S1). Because neurons

of the entopeduncular nucleus (EPN) and ventral tegmental area (VTA) co-release glutamate (40, 41) and because the LHb-projecting SVTg (SVTg→LHb) neurons are not glutamatergic (as below), the SVTg represents by far the largest purely GABAergic input nucleus to the LHb (fig. S1B).

Using immunohistochemistry on coronal and sagittal brain slices, we found that SVTg→LHb GABAergic neurons are clearly separated from adjacent laterodorsal tegmentum (LDTg), locus coeruleus (LC) and dorsal raphe (DR) neuronal populations (Fig. 1, C to F, fig. S1, F and G, figs. S2 and S3, and movie S1). We found that the SVTg extends far beyond the adjacent LDTg and dorsal tegmentum (DTg) both rostrally and caudally (Fig. 1, E and F, and fig. S1, F and G). SVTg projection to the LHb is mainly ipsilateral, whereas some SVTg→LHb neurons are in the midline (fig. S1, C to E).

The LHb-injected Cre-dependent retrograde AAV-labeled SVTg neurons in vGAT-Cre mice (fig. S4A), but not in choline acetyltransferase (ChAT)-Cre, vesicular glutamate transporter 2 (vGluT2)-Cre, or somatostatin (SOM)-Cre mice (fig. S4, B and D), demonstrating that SVTg→LHb neurons are not cholinergic, glutamatergic, or somatostatin-positive. Injection of the same retrograde AAV into brain areas adjacent to the LHb provided no labeling in the SVTg in vGAT-Cre mice (fig. S4, E to H).

Using Cre-dependent and -independent double retrograde viral tract tracing, we found that almost all SVTg→LHb neurons are GABAergic in the SVTg (fig. S5, A to C). However, SVTg neurons were negative for many other known markers of the PCG neurons (fig. S5, D to K). These data revealed the GABAergic population forming the SVTg in the PCG, which provides the largest purely inhibitory input to the LHb.

The SVTg densely innervates the LHb with GABAergic synapses

Using intersectional viral tract-tracing methods (Fig. 1G and fig. S6, A and B), we selectively visualized the distribution of SVTg fibers in the LHb. We found that the SVTg densely innervates the entire rostro-caudal extent (dominantly the medial and posterior part) of the LHb (Fig. 1H and fig. S6, C and D). Almost all of these axons in the LHb were positive for vGAT, but not for transporters of excitatory transmitters (fig. S6, E to G). The axon collaterals of the same SVTg→LHb neurons also targeted other memory formation- and valence processing-related subcortical regions (Fig. 1, O to Q).

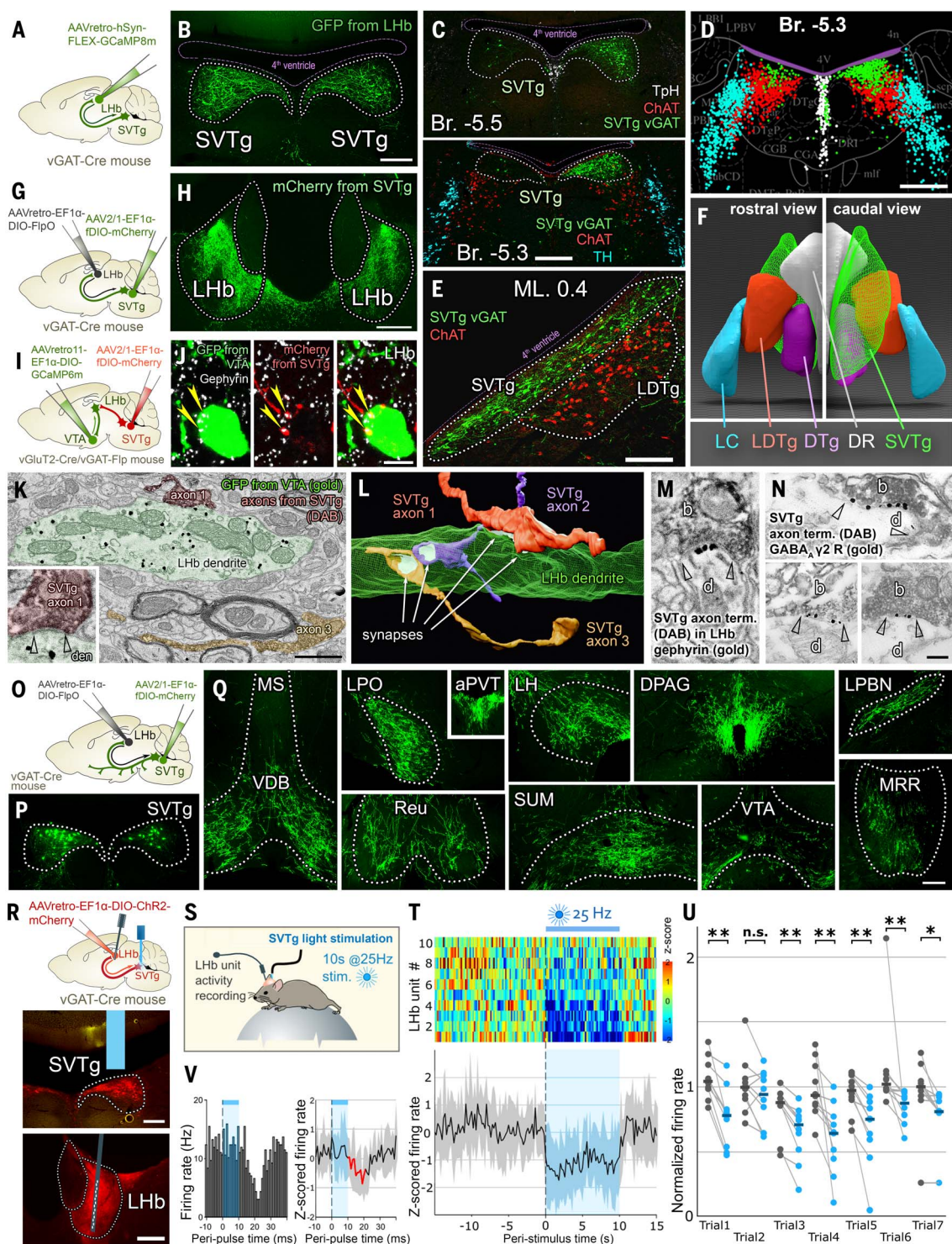
LHb neurons broadcast the negative valence signal to the VTA (4, 5, 17). To investigate whether the VTA-projecting LHb (LHb→VTA) neurons are directly inhibited by SVTg→LHb neurons, we performed combined, anterograde, and retrograde viral tract tracing experiments. We found that SVTg neurons established gephyrin-positive contacts with the somata and dendrites

¹Laboratory of Cerebral Cortex Research, HUN-REN Institute of Experimental Medicine, Budapest, Hungary. ²János Szentágothai Doctoral School of Neurosciences, Semmelweis University, Budapest, Hungary. ³Tamás Roska Doctoral School of Sciences and Technology, Pázmány Péter Catholic University, Budapest, Hungary. ⁴Laboratory of Cellular Neuropharmacology, HUN-REN Institute of Experimental Medicine, Budapest, Hungary. ⁵Laboratory of Neural Connectivity, Brain Research Institute, Faculties of Medicine and Science, University of Zurich, CH-8057 Zurich, Switzerland. ⁶Laboratory of Translational Behavioral Neuroscience, HUN-REN Institute of Experimental Medicine, Budapest, Hungary.

*Corresponding author. Email: nyiri.gabor@koki.hun-ren.hu

Fig. 1. The pontine SVTg inhibits LHb with GABAergic synapses.

(A) and (B) Cre-dependent GCaMP8m(GFP)-expressing retrograde AAV was injected into the LHb of four vGAT-Cre mice bilaterally, labeling the SVTg (B). Scale bar, 200 μ m. (C) Unilateral LHb injection of the same AAV, labeling SVTg neurons (green), distinct from TH-positive LC (cyan), ChAT-positive LDTg (red), and TpH-positive DR (white) neurons (see also figs. S1 to S3). Scale bar, 300 μ m. (D) Localizations of adjacent nuclei at section Bregma (Br.) 5.3 mm. Scale bar, 500 μ m. (E) Sagittal section shows the SVTg (green) and the neighboring cholinergic LDTg (red). Scale bar, 200 μ m. (F) 3D reconstruction of the SVTg and the surrounding nuclei (DR, LDTg, DTg, LC). See also movie S1. (G) and (H) A Cre-dependent Flippase-expressing retrograde AAV (colorless) was injected into the LHb, and a Flippase-dependent mCherry-expressing AAV was injected into the SVTg of four vGAT-Cre mice. mCherry labeling revealed (H) abundant SVTg innervation of the LHb (green). Scale bar, 200 μ m. (I) and (J) Cre-dependent GCaMP6m(GFP)-expressing retrograde AAV was injected into the VTA, and a Flippase-dependent mCherry-expressing AAV was injected into SVTg of three vGluT2-Cre/vGAT-Flp double transgenic mice. SVTg fibers (J) (red) establish gephyrin (white) positive putative synaptic contacts (yellow arrowheads) with the soma of VTA-projecting glutamatergic LHb cells (green). Scale bar, 10 μ m. (K) Electron micrograph shows a synaptic contact (synaptic edges marked with open arrowheads in inset) established by an SVTg terminal (DAB precipitate, red, axon 1) on a VTA-projecting LHb glutamatergic cell dendrite (retrogradely labeled from VTA, immunogold labeling in four mice, green). Scale bar, 1 μ m. Inset scale bar is in (N) (L) 3D reconstruction of SVTg axons (axons 1 and 3 same as in Fig. 1K) showing their synapses (white) with a dendrite of an LHb neuron. The dendritic membrane was made partially transparent to reveal the synapses on the other side of the dendrite. (M) and (N) GFP-labeled SVTg boutons (b, DAB precipitate) establish synapses (edges, open arrowheads) on dendrites (d) that



contain gephyrin [gold particles, in two mice (M)] and GABA_A receptor $\gamma 2$ -subunit [gold particles, in two mice (N)]. Scale bar, 200 nm [applies to (M), (N), and the inset of (K)]. (O) Cre-dependent Flp-expressing colorless retrograde AAV (AAVretro-EF1 α -DIO-FlpO) was injected into the LHb, and Flp-dependent fluorescent protein-expressing AAV (AAV2/1-EF1 α -fDIO-mCherry) was injected into the SVTg of 4 vGAT-Cre mice. (P) SVTg GABAergic neurons labeled using intersectional viral tracing methods according to (O). (Q) Representative fluorescent images show the axon collaterals of SVTg \rightarrow LHb neurons in different brain regions. Scale bar for (P) and (Q), 200 μ m. (R) Cre-dependent Chr2-mCherry-expressing retrograde AAV was injected into the LHb of vGAT-Cre mice,

and an optic fiber was implanted over the SVTg. Then, a silicon probe was inserted into the Lhb. Fluorescent images show the position of the optic fiber (blue) and viral expression in the SVTg (top) and the position of the silicon probe (gray) in the Lhb (bottom). Scale bars, 200 μ m. (S) Experimental design for the *in vivo* electrophysiological recording experiment. Head-restrained mice received 10-s, 25-Hz laser-stimulation (10 ms pulse length), while Lhb unit activities were recorded. (T) Z-scored peri-stimulus time histograms of Lhb units with firing rate reduction during 10-s, 25-Hz stimulation (top), with the corresponding average peri-stimulus time histogram (bottom, mean \pm s.dev.). Blue shaded areas indicate the duration of light exposure. (U) Paired plots of baseline normalized to the corresponding average baseline firing

rates of Lhb units (a unit represents a single cell in Lhb, same units as in Fig. 1T) during repeated laser stimulation trials (gray, average firing rates of 10-s baseline periods, blue, average firing rates of 10-s laser stimulation periods, $n = 10$ units from four mice) (V) Peri-stimulus time histogram shows the averaged response of a sample Lhb unit to the repeated 10-ms laser pulses (left). Averaged z-scored peristimulus time histogram of the Lhb units with significant ($P < 0.05$) responses to the repeated 10-ms laser pulses [(right) mean \pm s.dev.] Blue horizontal bars and shaded areas indicate the duration of light exposure. The red segment indicates significant ($P < 0.05$) firing rate reduction ($n = 7$ units from four mice). For statistical details, see table S2. For reconstructed injection site, probe, and optic fiber localization, see fig. S20.

of Lhb \rightarrow VTA neurons (Fig. 1, I and J, and fig. S6, H to K). Electron microscopy revealed that the SVTg forms typical GABAergic symmetrical synapses with Lhb \rightarrow VTA neurons (out of 59 randomly collected synapses of SVTg axons, 47 targeted dendritic shafts and 12 targeted spines in four mice; Fig. 1, K and L) and that SVTg synapses contain both GABA_A-receptor γ 2-subunits and gephyrin postsynaptically in the Lhb (Fig. 1, M and N). Our measurement showed that at least 31 out of 32 synapses contained γ 2-subunit of the GABA_A-receptor labeling and at least 20 out of 25 synapses contained gephyrin (Fig. 1, M and N). These results demonstrate a circuit-specific inhibition of the Lhb by SVTg neurons.

The SVTg inhibits Lhb neurons *in vivo*

To investigate the functional connectivity between SVTg and Lhb neurons, we used a combination of *in vivo* multichannel electrophysiological recordings and optogenetic stimulations in awake head-fixed mice. We infected SVTg neurons retrogradely from the Lhb with a channelrhodopsin 2 (ChR2)-expressing, Cre-dependent AAV in vGAT-Cre mice, and implanted an optical fiber over the SVTg (Fig. 1R). Lhb unit activity was recorded by using a 128-channel silicone probe parallel with optogenetic activation of the SVTg (Fig. 1S). Even though it is not possible to activate all SVTg neurons effectively, we found that at least 23% (10 out of 44) Lhb neurons decreased their activity consistently in response to the optogenetic stimulation of SVTg neurons (Fig. 1, T and U, fig. S7A, and table S2). Furthermore, the response latencies of Lhb units revealed a very fast reduction of firing rates following the 10-ms laser pulses, within the 10-to-20-ms time window after the laser pulse onset (Fig. 1V, fig. S7B, and table S2). We also found that the SVTg could inhibit typical Lhb units that were activated by aversive airpuffs (fig. S7, C and D). These results demonstrate that the SVTg can directly inhibit the Lhb neurons, which participate in encoding negative experiences.

SVTg stimulation is rewarding

Because inhibition of the Lhb can induce a rewarding experience (21, 35, 37), we tested the effect of optogenetic stimulation of the SVTg in behavioral experiments. Again, we infected

SVTg \rightarrow Lhb neurons in vGAT-Cre mice, with a ChR2 expressing AAV (ChR2 mice) or a control AAV (CTRL mice). We then implanted optic fibers above the SVTg (Fig. 2A). After handling, we conducted real-time place preference (RTPP) and conditioned place preference (CPP) tests on separate days (Fig. 2B). On the habituation day, mice showed no preference for either chamber of the double-chamber box (Fig. 2C and fig. S7E). The next day, mice received continuous light exposure when they entered one of the chambers. We tested light stimulations at 4 and 20 Hz in two independent cohorts to better understand the frequency dependence of the effects. In contrast to CTRL mice, ChR2 mice (using both 4 and 20 Hz) showed a strong, immediate RTPP for the stimulated chamber of the double-chamber box (Fig. 2, C and D, fig. S7, E and F, and table S3). The velocity changes of the ChR2 mice during the RTPP tests may suggest reward-seeking behavior (fig. S7G).

The following day, the mice were returned to the double-chamber box without light exposure. ChR2 mice that previously received 20-Hz stimulations, but not CTRL and ChR2 mice that previously received 4-Hz stimulations, showed place preference for the chamber in which they were previously stimulated (Fig. 2, C and D, fig. S7, E and F, and table S3).

To prove that SVTg fibers targeting the Lhb are directly responsible for inducing place preference behavior, we performed a similar experiment but stimulated SVTg fibers in the Lhb only (Fig. 2E) and performed the same RTPP and CPP experiments as above. Again, we found that, in contrast to CTRL mice, ChR2 mice showed strong RTPP and CPP towards the chamber of the box where they received the stimulation (Fig. 2F and table S3).

Mice self-stimulate their SVTg

To test whether mice are willing to actively work for the activation of SVTg neurons, we performed an optogenetic self-stimulation experiment. SVTg \rightarrow Lhb neurons were infected in vGAT-Cre mice, with a ChR2 expressing (ChR2 mice) or a control AAV (CTRL mice). We then implanted optic fibers above the SVTg (Fig. 2G). Food-restricted mice were trained for 10 days in an operant conditioning task with two nose-poke holes. Mice received light exposure only

when they poked their noses into the predefined (ILLUM) holes (Fig. 2H). We found that ChR2 mice poked their noses into the ILLUM hole more than CTRL mice, so much so that by the last day of training (day 10), ChR2 mice poked their noses into the ILLUM hole more than eight times as often than CTRL mice (Fig. 2I and table S3). ChR2 mice also preferred the ILLUM hole (fig. S7, H and I, and table S3).

Finally, we tested the memory of the preference of ChR2 mice in the absence of light exposure and found that they still preferred the ILLUM hole more than the CTRL mice (Fig. 2, I and J, fig. S7, H and I, and table S3). These results suggest that SVTg activation exerts a rewarding effect and that mice try to self-activate their SVTg, even when the ILLUM hole did not trigger light stimulation, suggesting a role of the SVTg in reward-seeking behavior.

SVTg stimulation is anxiolytic

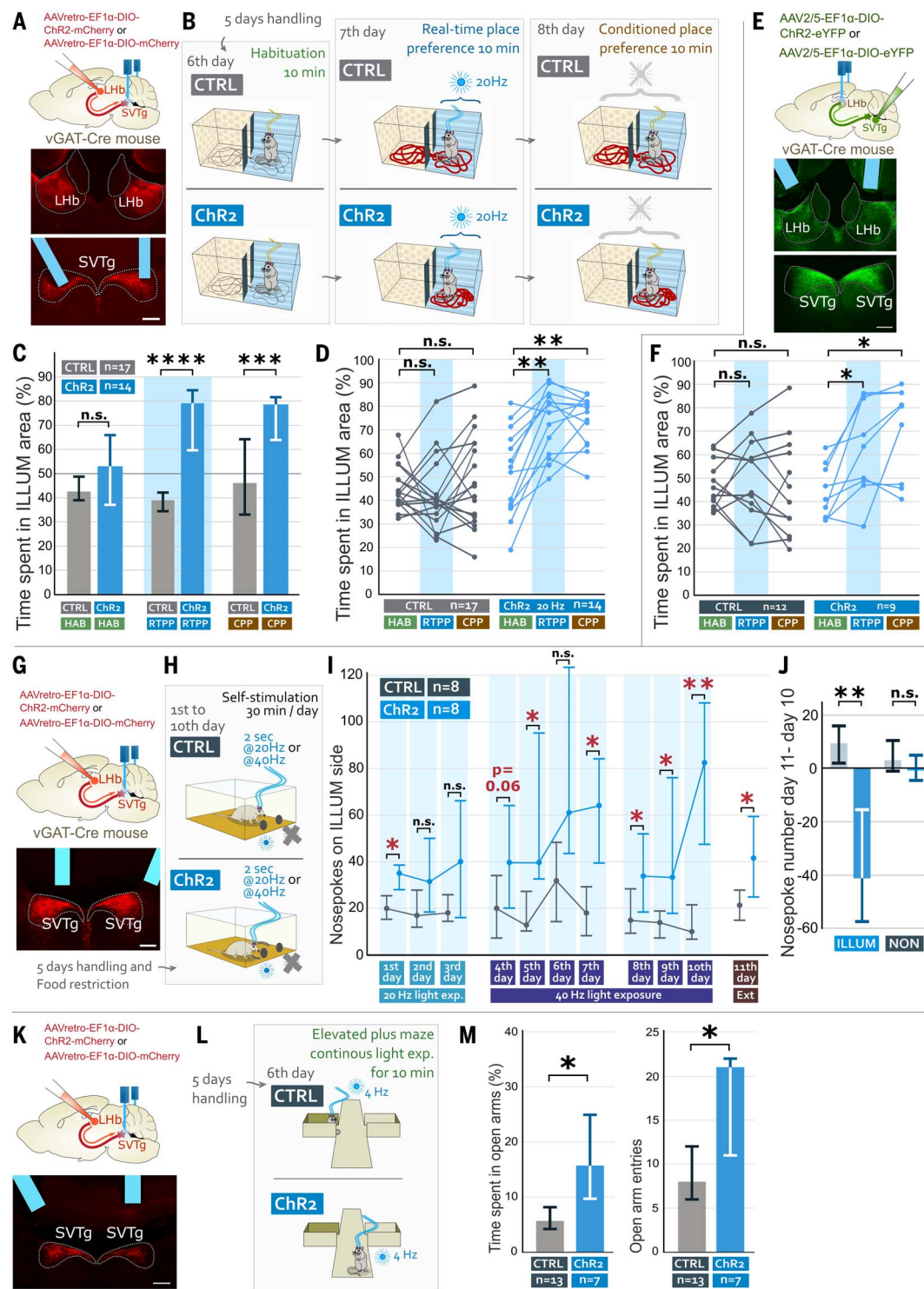
The innate fear of open, elevated platforms induces anxious behavior in mice which is also controlled by the valence circuitry. We investigated whether optogenetic activation of the SVTg could reduce anxiety in mice. We infected SVTg \rightarrow Lhb neurons in vGAT-Cre mice, with a ChR2 expressing (ChR2 mice) or a control AAV (CTRL mice). We then implanted optic fibers above the SVTg (Fig. 2K). We placed ChR2 and CTRL mice onto an elevated plus maze (EPM), where they received continuous 4-Hz light exposure for 10 minutes during the entire experiment (Fig. 2L). ChR2 mice spent more time in the open arms and had a higher number of entries into the open arms than CTRL mice (Fig. 2M and table S3) suggesting that SVTg activation might exert anxiolytic effects.

SVTg stimulation increases accumbal dopamine release

Dopamine release in the nucleus accumbens (NAcc) can signal a rewarding experience (4, 43). Although the SVTg does not project to the NAcc directly (Fig. 1Q), we investigated whether the SVTg can regulate reward processing through the known Lhb \rightarrow VTA \rightarrow NAcc axis (44, 45). We infected SVTg \rightarrow Lhb neurons in vGAT-Cre mice with a ChR2-expressing AAV. Then, dopamine-indicator photosensors (DA4.4-GRAB_{DA}) were expressed in the NAcc using another AAV. We implanted an optic fiber above the SVTg for

Fig. 2. SVTg neurons induce rewarding experiences in mice.

(A) We injected Cre-dependent retrograde AAVs that either expressed ChR2 (ChR2 mice) or did not express ChR2 (CTRL mice) into the Lhb of vGAT-Cre mice and implanted optic fibers over the SVTg, bilaterally. Fluorescent images show the injection sites in the Lhb and the position of the optic fibers (blue) and retrograde labeling of SVTg neurons (red). Scale bar, 200 μ m. (B) After handling, mice were habituated (HAB) to a box with two chambers. On day 7, mice received 20-Hz optical fiber light exposure in one of the chambers to test real time place preference (RTPP). On day 8, the conditioned place preference (CPP) of mice was tested in the same box without light exposure. (C) The graph shows that, compared with non-stimulated CTRL mice, ChR2 mice spent significantly more time in the chamber associated with SVTg-stimulation, showing both RTPP and CPP (medians and interquartile ranges). (D) Chamber preference of individual mice during days 6 (HAB), 7 (RTPP), and 8 (CPP) of the experiment. (E) We bilaterally injected Cre-dependent anterograde AAVs with (ChR2 mice) or without the expression of ChR2 (CTRL mice) into the SVTg of vGAT-Cre mice, and optic fibers were implanted over the Lhb, bilaterally. The images show the injection site in the SVTg and the position of the optic fibers (blue) over the Lhb. Scale bar, 200 μ m. The same behavioral experiment was performed as described in (B) but here we exposed the fibers of the SVTg to light in the Lhb. (F) Chamber preference of individual mice during days 6 (HAB), 7 (RTPP), and 8 (CPP) of the experiment. (G) For self-stimulation experiments, injection sites, viruses, and optic fiber positions were identical to those in Fig. 2A. Scale bar, 200 μ m. (H) After handling, food-restricted CTRL and ChR2 mice were placed into a chamber containing two nose-poke holes. Tests lasted for ten days, 30 minutes each day. Mice received 2-s 20-Hz and later 40-Hz light exposure when they inserted their noses into the predefined hole (ILLUM side). (I) The graphs show that the ChR2 mice stuck their noses significantly more into the hole, where they received light exposure (ILLUM side), compared to CTRL mice on several different days. Experimental days were consecutive days except for experimental day 8 that started 2 weeks after day 7 (medians and interquartile ranges). (J) The graph shows the differences in the number of nose-pokes between days 11 and 10 on the light



exposed (illuminated, ILLUM) and not-light-exposed [non-illuminated (NON) holes] (medians and interquartile ranges). (K) For anxiety tests, injection sites, viruses, and optic fiber positions were identical to that in Fig. 2, A and G. Scale bar, 200 μ m. (L) Experimental design for elevated plus maze (EPM) experiments. CTRL and ChR2 mice were placed on an EPM and received 4-Hz optic fiber light exposure for 10 minutes. (M) Graphs show differences between CTRL and ChR2 mice in time spent in the open arms and open arm entries (medians and interquartile ranges). For statistical details, see table S3. For reconstructed injection site and optic fiber localization see fig. S20.

optogenetic stimulation and another optic fiber above the NAcc for recording dopamine release using fiber photometry in awake mice (Fig. 3A). Although several other pathways can modulate dopamine release, we found that activation of the SVTg could also elicit a dopamine release in

the NAcc (Fig. 3, B and C, fig. S8, C and D, and table S4) that was similar to that induced by the water reward in water-restricted mice (Fig. 3C and fig. S8, A to D). These results further confirmed that the SVTg could modulate dopamine-mediated reward processing.

SVTg neurons are rapidly activated by rewarding events

To test whether natural reward triggers immediate-early gene expression in SVTg neurons, we investigated c-Fos expression of SVTg neurons in food-restricted mice after a food reward. First,

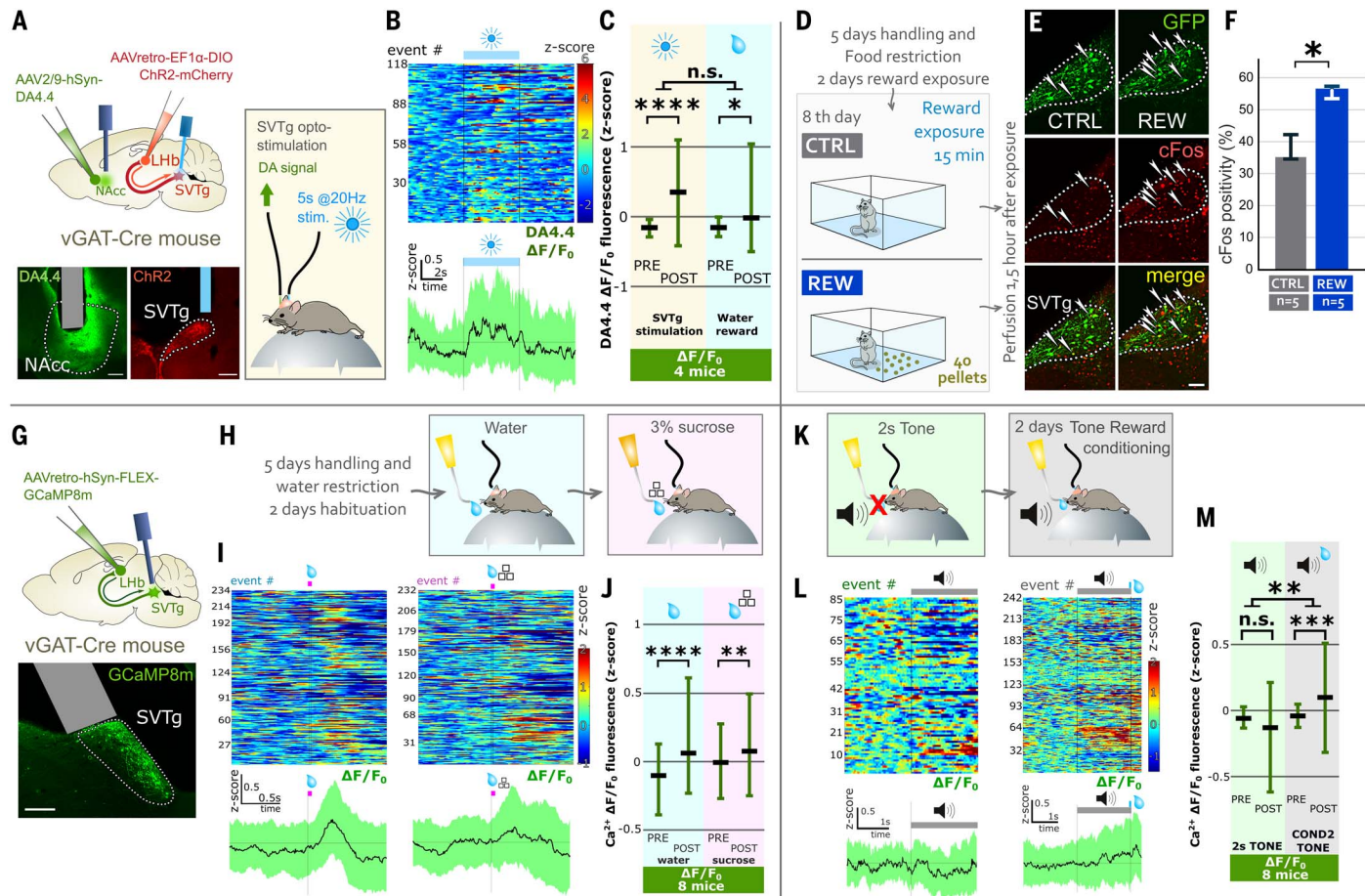


Fig. 3. The SVTg induces dopamine release in the NAcc and is activated by rewarding experiences. (A) Dopamine sensor (DA4.4)-expressing AAV was injected into the NAcc and ChR2-expressing Cre-dependent retrograde AAVs were injected into the LHB of vGAT-Cre mice. Optic fibers were implanted over the SVTg and NAcc. Fluorescent images show the injection sites and the placement of optic fibers (gray and blue) into the NAcc and SVTg. Scale bars, 200 μ m. Mice received 20-Hz, 5-s optical stimulation of the SVTg randomly, several times, while DA-release was detected in the NAcc. (B) (Top) Heatmap plot showing changes in the $\Delta F/F$ -signal after SVTg optical stimulation in all events ($n = 118$). (Bottom) Perievent plot shows medians and interquartile ranges of $\Delta F/F$ change in responding to SVTg optical stimulation. (C) Graph shows significant changes in the $\Delta F/F$ signals both after SVTg optical stimulation and during water reward consumption from four mice (medians and interquartile ranges). (D) GFP-expressing Cre-dependent retrograde AAVs (AAVretro-hSyn-FLEX-GCaMP8m) were injected into the LHB of vGAT-Cre mice to label their SVTg. REW mice then received a food reward while CTRL mice did not. (E) Representative fluorescent images of the SVTg of CTRL and REW mice show that reward induced a strong expression of c-Fos (red) in GFP-labeled SVTg neurons (green). White arrowheads indicate double-positive neurons. Scale bar, 100 μ m. (F) Graph shows significant difference in c-Fos positivity of SVTg neurons between CTRL and REW mice (medians and interquartile ranges). (G) GCaMP8m-expressing Cre-dependent retrograde AAVs were injected into the LHB of vGAT-Cre mice to

label SVTg neurons, and an optic fiber was implanted over the SVTg. Sagittal fluorescent image shows the viral expression (green) and optic fiber (gray) position in the SVTg. Scale bar, 200 μ m. (H) Water-restricted mice received pure water or sweet water droplets and the Ca^{2+} -activity of SVTg neurons was recorded. (I) (Top) Heatmap plots show changes in the $\Delta F/F$ signal recorded from mice that received water (left) ($n = 234$ events) or sweet (sucrose) water (right) ($n = 232$ events). (Bottom) Perievent plots show medians and interquartile ranges of $\Delta F/F$ changes in response to water (left) or sweet water (right) reward. (J) Graph shows significant changes in the $\Delta F/F$ signals after water or sweet water droplet delivery in eight mice (medians and interquartile ranges). (K) Mice were exposed to neutral tones (2-s tone), which did not alter SVTg activity by themselves. Tones were then co-terminated with water rewards for 2 days and SVTg activity was recorded during the second conditioning day (COND2 TONE). (L) (Top) Heatmap plots show changes in the $\Delta F/F$ signal in events from mice during a 2-s TONE (left) ($n = 85$ events) or COND2 TONE (right) ($n = 242$ events). (Bottom) Perievent plots show medians and interquartile ranges of $\Delta F/F$ change in response to a 2-s TONE (left) or COND2 TONE (right). (M) Graph showing that the SVTg was significantly activated by the reward associated TONE, compared to both the control TONE and its activity immediately before the tone from eight mice (medians and interquartile ranges). For statistical details, see tables S3 and S4. For reconstructed injection site and optic fiber localization, see fig. S20.

we infected SVTg \rightarrow LHb neurons in vGAT-Cre mice with GFP-expressing AAV. After food restriction, a subgroup of these mice received sucrose reward pellets in a new context (REW mice), whereas another subgroup of mice (CTRL mice) was placed into the same new context without reward pellets (Fig. 3D). We found that the reward induced increased c-Fos activity in the SVTg of REW mice compared with CTRL mice (Fig. 3, E and F, and table S3).

To test the timing of the SVTg neuronal response to the reward, we performed a fiber photometry calcium imaging experiment. We infected SVTg \rightarrow LHb neurons in vGAT-Cre mice with a calcium-indicator protein (GCaMP8m)-expressing AAV. We then implanted an optic fiber above the SVTg to detect the activity of its labeled neurons (Fig. 3G). We found that the water reward (both pure and water droplets containing sucrose) induced an increase in neuronal activity in SVTg neurons of trained,

head-restrained, water-restricted mice (Fig. 3, H to J, and table S4). Calcium imaging showed that the activation of SVTg neurons occurred quickly, broadcasting the reward signal within a few hundred milliseconds after natural reward presentation, whereas no changes were detected in control (isosbestic) signals (Fig. 3, H to J, and fig. S8, E and F).

The SVTg signals reward prediction

To investigate whether the expectation of a reward also activates SVTg neurons, we used fiber photometry. We used the same cohorts of mice described in the previous section, where SVTg \rightarrow LHb neurons expressed GCaMP8m. First, we found that the effects of neutral stimuli (such as pure tones or short or long ambient light illuminations) did not activate SVTg neurons in head-restrained mice (Fig. 3, K to M, fig. S8, G to M, and table S4). At the beginning of the subsequent experiment (day 1), water-restricted

mice were trained to learn that they would always receive a water drop at the end of a 2-s tone presentation (Fig. 3K). On day 2 (COND2), we found that reward-predicting tones increased the activity of SVTg neurons without affecting the control (isosbestic) signals (Fig. 3, L and M, fig. S8, L and M, and table S4). These results suggest that SVTg activity likely predicts reward.

The SVTg can regulate reward location memory

Remembering the location of previously found food requires the assignment of reward attributes to food locations. To test the SVTg in these processes, we used a food-induced place preference paradigm. We specifically infected SVTg neurons with an inhibitory, soma-targeted, *Guillardia theta* anion-conducting, channelrhodopsin 2-expressing (stGtACR2 mice) or a control AAV (CTRL mice); we also implanted optic fibers above the SVTg (Fig. 4A). After handling

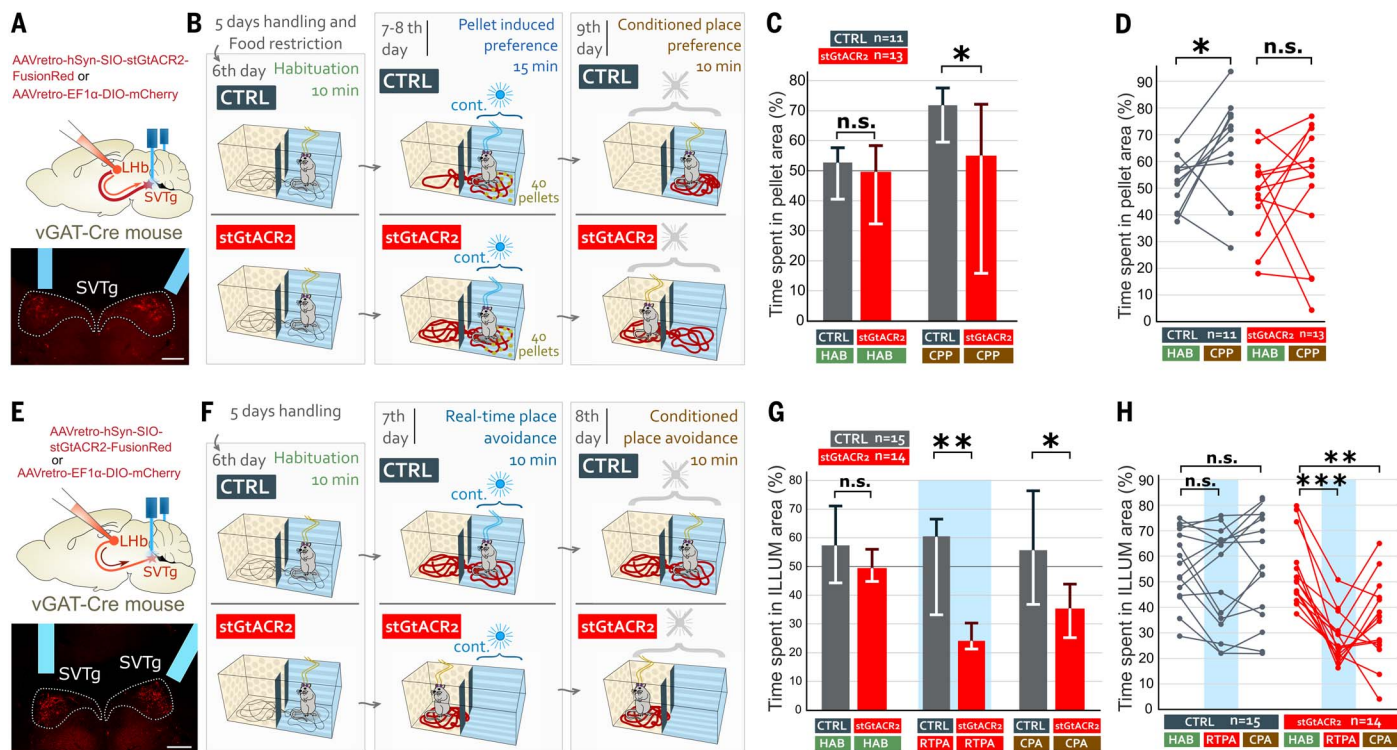


Fig. 4. Inhibition of the SVTg disrupts food-induced preference learning and induces avoidance. (A) We injected Cre-dependent retrograde AAVs that either expressed the inhibitory opsin stGtACR2 (stGtACR2 mice) or did not express the stGtACR2 (CTRL mice) into the LHb of vGAT-Cre mice. Both viruses contained a reporter protein. Then, we implanted optic fibers over the SVTg, bilaterally. Fluorescent image shows an example position of the optic fibers (blue) and the retrogradely labeled SVTg neurons (red). Scale bar, 200 μ m. (B) After 5 days of handling and food restriction, mice were habituated (HAB) to a dual-chamber box. On day 7 and 8, 40 pellets were placed into one chamber of the box (for inducing a food-reward induced preference). In the same chamber mice received continuous light exposure. On day 9, mice were placed back into the dual-chamber box, without any pellet and without any optic fiber light exposure to test their conditioned place preference (CPP). (C) Graphs show that mice did not prefer any of the chambers during habituation (HAB). However, during CPP test, unlike CTRL mice,

stGtACR2 mice did not prefer the reward-associated chamber (medians and interquartile ranges). (D) Pairwise comparisons also show that unlike CTRL mice, stGtACR2 mice did not change their preference for the reward-associated chamber. (E) For place avoidance tests, we prepared mice the same way and using the same AAVs as in Fig. 4A. Scale bar, 200 μ m. (F) After 5 days of handling, mice were habituated (HAB) to a dual-chamber box. On day 7, mice received continuous optic fiber light exposure for 10 min, to test their potential real time place avoidance (RTPA). On day 8, mice were placed back into the same box, but without light exposure, to test their potential conditioned place avoidance (CPA). (G) Graphs show that mice did not prefer any of the chambers during habituation (HAB). stGtACR2, but not CTRL mice demonstrated significant RTPA and CPA (medians and interquartile ranges). (H) Pairwise comparisons also show that unlike CTRL mice, stGtACR2 mice avoided the chamber significantly more where their SVTg was inhibited. For statistical details, see table S3. For reconstructed injection site and optic fiber localization see fig. S20.

and controlled food restriction, mice were placed into a double-chamber box for habituation (day 6), where neither CTRL nor stGtACR2 mice showed place preference (Fig. 4, B and C). On days 7 and 8, mice received 40 sucrose-containing pellets in only one of the chambers, where their SVTg were also exposed to light (Fig. 4B). By day 2, the stGtACR2 mice showed lower preference for the pellet-containing-chamber compared with CTRL mice (fig. S8, N and O, and table S3).

On day 9, mice received no pellets and no optic fiber light exposure, and we tested their place preference (Fig. 4B). CTRL mice showed place preference for the previous food location, whereas stGtACR2 mice did not (Fig. 4, C and D, and table S3), suggesting that normal activity of the SVTg is necessary for reward location memory.

Basal activity of the SVTg is required for a balanced assessment of valence

Using optogenetic inhibition, we investigated whether the activity of the SVTg is necessary for a balanced valence circuit. We infected SVTg→LHb neurons in vGAT-Cre mice with inhibitory stGtACR2-expressing (stGtACR2 mice) or a control (CTRL mice) AAV before implanting optic fibers over the SVTg (Fig. 4E). After handling, neither CTRL nor stGtACR2 mice showed place preference in a neutral double-chamber box (Fig. 4, F and G). The following day, mice were placed back into the same box and their SVTg was exposed to light continuously in only one of the chambers. In contrast to CTRL mice, stGtACR2 mice showed immediate real time place aversion (RTPA) for the SVTg-inhibited chamber (Fig. 4, G and H, and table S3); they also exhibited decreased movement in the non-inhibited chamber, suggesting passive avoidance of the other chamber (fig. S8P).

The following day, all mice were placed back into the same dual-chamber box without light exposure. In contrast to CTRL mice, stGtACR2 mice showed conditioned place aversion (CPA) of the chamber, where their SVTg neurons were previously inhibited (Fig. 4, G and H, and table S3). The results suggest that the SVTg likely has a baseline neuronal activity that maintains a healthy valence detection and motivational state during spatial exploration.

Precisely timed activity of SVTg neurons prevents excessive fear response

Fearful events require powerful control of valence processing, including the mechanisms to prevent excessive fear responses during and after negative experiences. Because the SVTg keeps the assessment of valence under continuous control (Fig. 4, E to H) and has a fast response to reward (Fig. 3, G to J), we also investigated its role in balancing fear response. Using fiber photometry calcium imaging, we recorded neuronal activity of the SVTg during aversive events

(Fig. 5, A and B). SVTg→LHb neurons were labeled with a GCaMP8m-expressing AAV and a recording optic fiber was placed above the SVTg (Fig. 5A). We tested the same animals used for testing SVTg activity during reward processing (Fig. 3, G to J). First, we found that a mildly aversive, surprising, 1-s, random exposure to the sound of nearby airpuffs activated SVTg neurons (fig. S9, A and B, and table S4). However, if the same airpuffs were applied directly to the nose (highly aversive) of the head-restrained mice, they caused fast activation of SVTg neurons compared with both the control (isosbestic) signals and the sound of similar nearby airpuffs (Fig. 5, C to E, fig. S9, C and D, and table S4). Using a different group of mice, we found that 0.2-s direct air puffs, applied to the nose, elicited similar responses (fig. S9, E and F, and table S4).

Adaptation to a series of fearful events requires a continuous reevaluation of valence. The first fearful stimulus in a series must have a different valence than subsequent, less surprising stimuli. To investigate the involvement of the SVTg in such adaptation to 10 airpuff trains with random onsets, we monitored its activity using fiber photometry calcium imaging of GCaMP8m. We found that the initial five airpuffs caused stronger SVTg activation than the last five airpuffs within the trains (Fig. 5, F to H, and table S4). Additionally, the first three trains of airpuffs caused stronger SVTg activation than the last three trains (Fig. 5I, and table S4), whereas no similar difference was detected in the control (isosbestic) channel (fig. S9, G to I, and table S4). These intra- and inter-train accommodations suggest fast adaptations and plastic changes within the SVTg-related circuit or within SVTg neurons.

To investigate whether such fast natural activation of SVTg neurons was necessary to prevent excessive fear responses, we tested how mice coped with fear, without the activity of SVTg neurons. We infected SVTg→LHb neurons in vGAT-Cre mice with inhibitory stGtACR2-expressing AAV (stGtACR2 mice) or control AAV (CTRL mice). We then implanted optic fibers above the SVTg (Fig. 5J). All mice received four aversive foot shocks in context A (CTX-A), precisely aligned with a short, 6-s light exposure through optic fibers of SVTg neurons (Fig. 5J and fig. S9J). The following day, we placed the mice back in CTX-A and found that, unlike the CTRL mice, the stGtACR2 mice showed higher contextual fear responses (Fig. 5K and table S3). Later, we placed the mice into a novel context (CTX-B) to examine their generalized fear responses and we found that it was still increased in the stGtACR2 mice (Fig. 5K and table S3). These data show that the SVTg is necessary for controlling the strength of fear memory formation and preventing abnormal overgeneralization.

We also tested whether SVTg activation could suppress natural fear responses as well. We

infected SVTg→LHb neurons in vGAT-Cre mice, either with ChR2-expressing (ChR2 mice) or with a control AAV (CTRL mice). We then implanted optic fibers above the SVTg (fig. S9K). Mice received four foot shocks in CTX-A, aligned with a short, 5-s light exposure through optic fibers of SVTg neurons (fig. S9K). During this training, ChR2 mice (but not CTRL mice) already showed a suppressed intershock fear response (fig. S9L). The following day, we recorded the fear responses of these mice in CTX-A, and in a novel CTX-B. We found that ChR2 mice showed lower contextual fear in CTX-A, whereas the already very low fear response of CTRL mice in CTX-B could not be reduced further (fig. S9M and table S3). These data demonstrate that the SVTg is not only a positive valence center that broadcasts and controls reward, but it also plays a major role in counterbalancing the valence network during fear encoding.

SVTg neurons are targeted by motivation-related brain areas

To identify the brain areas that target SVTg neurons through direct synaptic connections, we used mono-transsynaptic rabies tracing. We infected SVTg neurons in vGAT-Cre mice directly with a Cre-dependent helper virus and injected a retrograde rabies virus into the LHb of the same mice (Fig. 6, A and B). We confirmed the specificity of these viruses (fig. S10, A and B).

We found that several key brain areas encoding valence, motivation, and aversion targeted SVTg GABAergic neurons monosynaptically (Fig. 6, C and D, and table S5), including the MRR, which plays a fundamental role in aversive behavior (23, 46). Our double tracing experiments revealed that MRR non-GABAergic (likely glutamatergic) (47) cells densely innervate the SVTg region and establish excitatory synaptic contacts with SVTg neurons (fig. S10, C to E). Additionally, we found that several higher-order associational cortical areas, such as the orbitofrontal cortex (OFC) and the anterior cingulate cortex, also targeted SVTg neurons (Fig. 6, C and D) and the avoidance-encoding IPN GABAergic neurons (48, 49) specifically innervate the SVTg with inhibitory synapses (fig. S10, F to H).

Cortical control of the SVTg

The activation of the SVTg by reward prediction (Fig. 3, K to M) suggested a regulation by higher-order associational cortices. Rabies tracing revealed such cortical inputs (Fig. 6, C and D); to confirm it, we infected cortical neurons retrogradely from one side of the SVTg of vGluT1-Cre mice (Fig. 6, E and F). We found that the OFC contained the largest number of retrogradely labeled pyramidal cells, whereas other higher-order associational cortices, including the anterior cingulate cortex and other prefrontal cortical regions, also targeted the SVTg (Fig. 6G and table S6).

Using combined anterograde and retrograde tracing, we found that OFC pyramidal cells

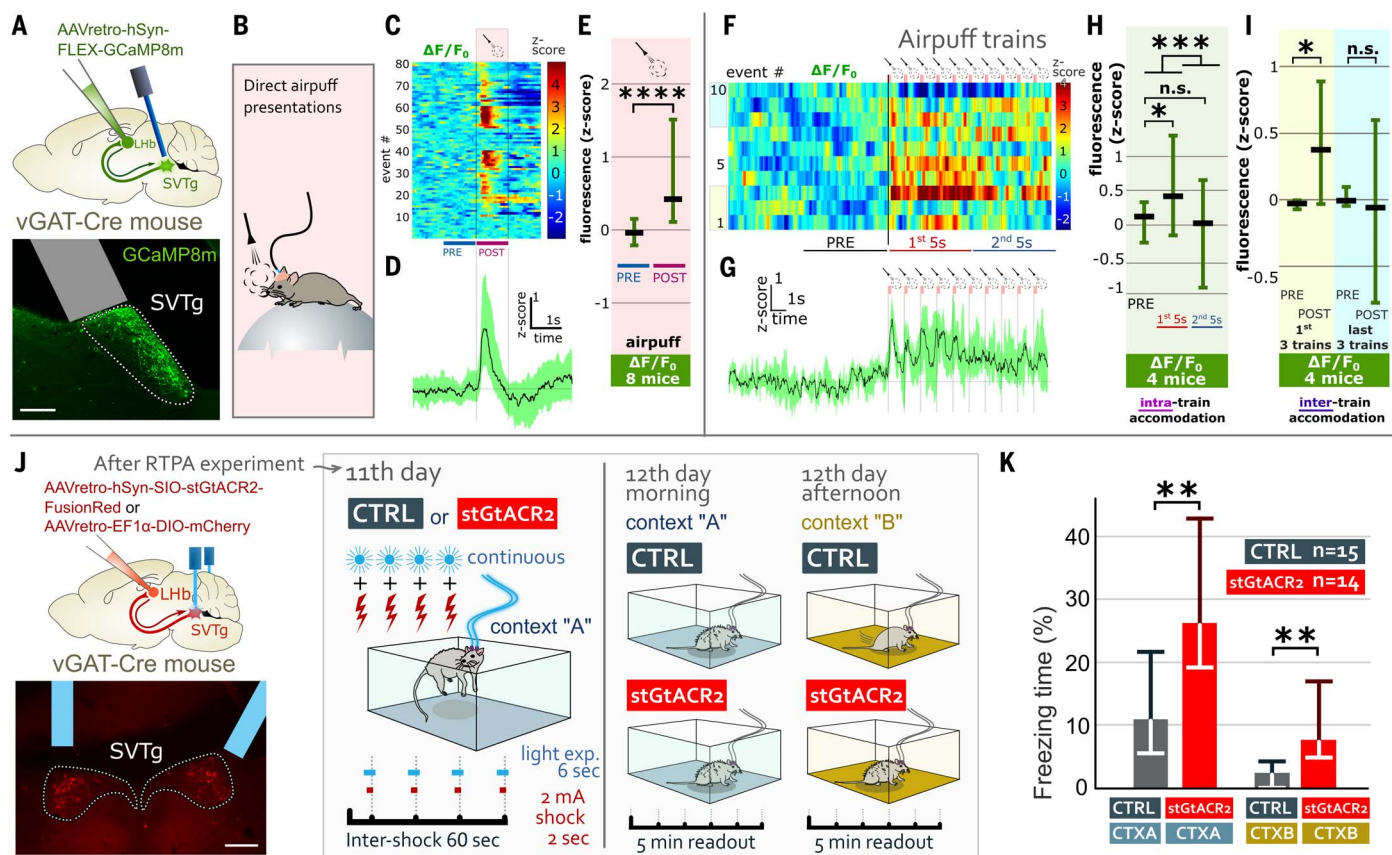


Fig. 5. SVTg neurons are activated by aversive events to control fear memory formation. (A) GCaMP8m(GFP)-expressing Cre-dependent retrograde AAVs were injected into the LHB of vGAT-Cre mice to label SVTg and an optic fiber was implanted over the SVTg. Sagittal fluorescent image shows the viral expression (green) and optic fiber (gray) position in the SVTg. Scale bar, 200 μm. (B) Experimental design of fiber photometry experiments, where mice received aversive airpuffs, while the Ca^{2+} -activity of SVTg neurons was recorded. (C) Heatmap plot shows changes in the $\Delta F/F_0$ signal recorded from 8 mice that received airpuffs ($n = 80$ events). (D) Perievent plot shows medians and interquartile ranges of $\Delta F/F_0$ change in response to airpuffs. (E) Graph shows significant changes in the $\Delta F/F_0$ signals after airpuff presentations from 8 mice (medians and interquartile ranges). (F) Heatmap plot shows changes in the $\Delta F/F_0$ signal from a representative example of a mouse that received ten consecutive airpuff trains (One train, 10 × 0.2 sec airpuffs in 10 s). (G) Perievent

plot shows medians and interquartile ranges of $\Delta F/F_0$ change in response to the airpuff trains from the same mouse (F). (H) and (I) Graph shows intra-train (H) and inter-train (I) accommodation of the changes in $\Delta F/F_0$ signals (40 events from four mice, medians and interquartile ranges). (J) For fear conditioning tests, we prepared mice the same way and using the same AAVs as in Fig. 4A. Scale bar, 200 μm. CTRL and stGtACR2 mice received four foot-shocks (2 mA, 2 sec) precisely aligned with light exposure via optic fibers (8–10 mW, 6 sec) of the SVTg in context A (CTXA). The next day, mice were placed back into CTXA and then into a different context B (CTXB), while their fear behaviors (freezing) were recorded. (K) Graphs demonstrate that SVTg inhibition (in stGtACR2 mice) during negative experiences significantly increases fear responses (freezing time) in both CTXA and CTXB (medians and interquartile ranges). For statistical details, see tables S3 and S4. For reconstructed injection site and optic fiber localization see fig. S20.

densely innervate the SVTg and form homer-1 positive synapses with SVTg neurons (fig. S10, I to L). Using immunohistochemistry, we found that at least 69% of SVTg neurons received, on average, about 4 to 5 synapses from the OFC (fig. S10L). Our correlated light and electron microscopic imaging confirmed that OFC synaptically targeted the dendrites and somata of SVTg neurons with excitatory axon terminals (fig. S10, M to O), suggesting that the SVTg likely plays a direct role in executing the reward-related higher-order OFC functions.

The SVTg mediates orbitofrontal cortex-induced reward processing

We also tested the role of SVTg-projecting OFC cells. We specifically infected vGluT1 neurons

of the OFC with either a ChR2-expressing (ChR2 mice) or a control AAV (CTRL mice) before implanting optic fibers over the SVTg (Fig. 6H). We performed the same place preference and fear conditioning experiments as for SVTg activation. However, here we tested the optogenetic stimulation of the OFC axon terminals in the SVTg (Fig. 6H). After handling, we performed RTPP and CPP tests on separate days (Fig. 6H). On habituation day, mice displayed no preference for any of the chambers of the double-chamber box (Fig. 6I). The following day, in the same dual-chamber box, mice received optogenetic light exposure in only one of the chambers. Unlike CTRL mice, ChR2 mice showed an immediate RTPP response to the stimulated side of the box (Fig. 6I and table S3). The following

day, mice were retested in the same double-chamber box without light exposure and again, ChR2 mice displayed an elevated CPP response for the location associated with the previously stimulated area (Fig. 6I and table S3).

Later, we optogenetically activated OFC axonal fibers in the SVTg of the same mice for 5 s right before three separate foot shocks in CTX-A (Fig. 6J and fig. S10P). The following day, we tested fear responses both in CTX-A and in a new CTX-B. We found that OFC fiber activation in the SVTg of ChR2 mice caused lower contextual fear in CTX-A, but no difference in generalized fear behavior in CTX-B compared with the CTRL mice (Fig. 6K and table S3). These experiments demonstrated that the OFC likely plays a role in valence processing through the SVTg.

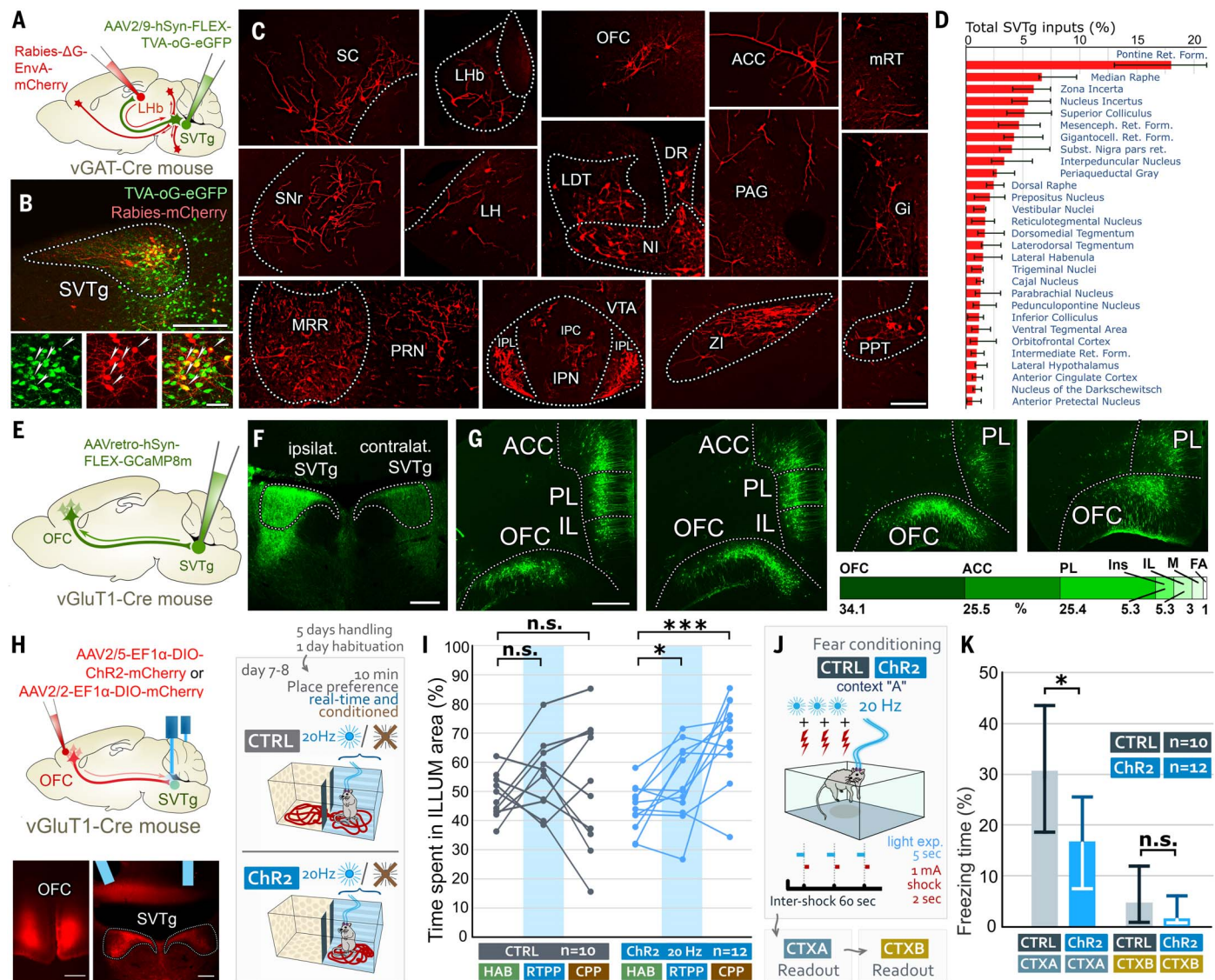


Fig. 6. Neuronal inputs of SVTg neurons. (A) Cre-dependent, avian receptor-expressing “helper” AAVs were injected into the SVTg, then 5 weeks later, avian receptor-dependent, mCherry-expressing, monosynaptically-restricted transsynaptic Rabies viruses were injected into the Lhb of five vGAT-Cre mice. (B) Fluorescent images show that yellow (white arrows) “starter” cells [that express both the helper (green) and rabies (red) virus products] are in the SVTg. Scale bar, 200 μ m (top), 20 μ m (bottom). (C) Representative fluorescent images show the retrogradely labeled monosynaptic inputs (red) of SVTg neurons. Scale bar, 200 μ m (D) Graph shows the ratio of neurons in brain areas that target the GABAergic neurons in the SVTg (medians and interquartile ranges, for details, see table S5). (E) GCaMP8m(GFP)-expressing Cre-dependent retrograde AAVs were injected into the SVTg unilaterally to label its cortical inputs in 2 vGluT1-Cre mice. (F) Image shows that injection into the SVTg unilaterally labeled vGluT1 positive frontal cortical neurons that targeted even the contralateral SVTg. Scale bar, 200 μ m. (G) Images show the cortical inputs of the SVTg and their ratio (for details, see table S6). Scale bar, 500 μ m. (H) We injected Cre-dependent anterograde AAVs

that either express ChR2 (ChR2 mice) or do not express ChR2 (CTRL mice) into the OFC of vGluT1-Cre mice and implanted optic fibers over the SVTg, bilaterally. A fluorescent image shows an example of the position of the optic fibers (blue) and the labeled OFC neurons and their fibers in the SVTg (red). Scale bars, 200 μ m. A 3-day-long place preference paradigm was performed with the CTRL and ChR2 mice. (I) Graph shows that unlike CTRL mice, ChR2 mice significantly preferred the chamber in which their OFC axonal fibers in the SVTg were stimulated in both RTPP and CPP days. (J) Then for further fear conditioning tests CTRL and ChR2 mice received three foot-shocks (1 mA, 2 sec) precisely preceded by 20 Hz optic fiber light exposure (8 to 10 mW, 5 sec, ending right before the foot-shock) of the SVTg in a CTXA. The next day, mice were placed back into CTXA and then into a different CTXB, while their fear behaviors (freezing) were recorded. (K) Graphs demonstrate that OFC fiber excitation (in ChR2 mice) significantly inhibits fear responses (decreases freezing time) in CTXA (medians and interquartile ranges). For statistical details, see table S3. For reconstructed injection site and optic fiber localization see fig. S20.

RNA sequencing reveals key reward-related receptors on SVTg neurons

The role of the SVTg is better understood by characterizing their inputs from neurotransmitter systems. Using the single-cell mRNA se-

quencing, we characterized the entire mRNA repertoire of SVTg GABAergic neurons (Fig. 7A). We confirmed the expression of GABAergic neuronal markers (GAD65, GAD67, GAT1, and vGAT), but not glutamatergic, cholinergic, or

monoaminergic markers (Fig. 7B). SVTg neurons highly expressed serotonin (Htr2c, Htr5a, Htr7), acetylcholine (Chrna3-5, Chrb2, Chrmb3), dopamine 1 (Drd1), cannabinoid 1 (Cnr1) and neuropeptide receptor genes (Oprl1, Oprk1,

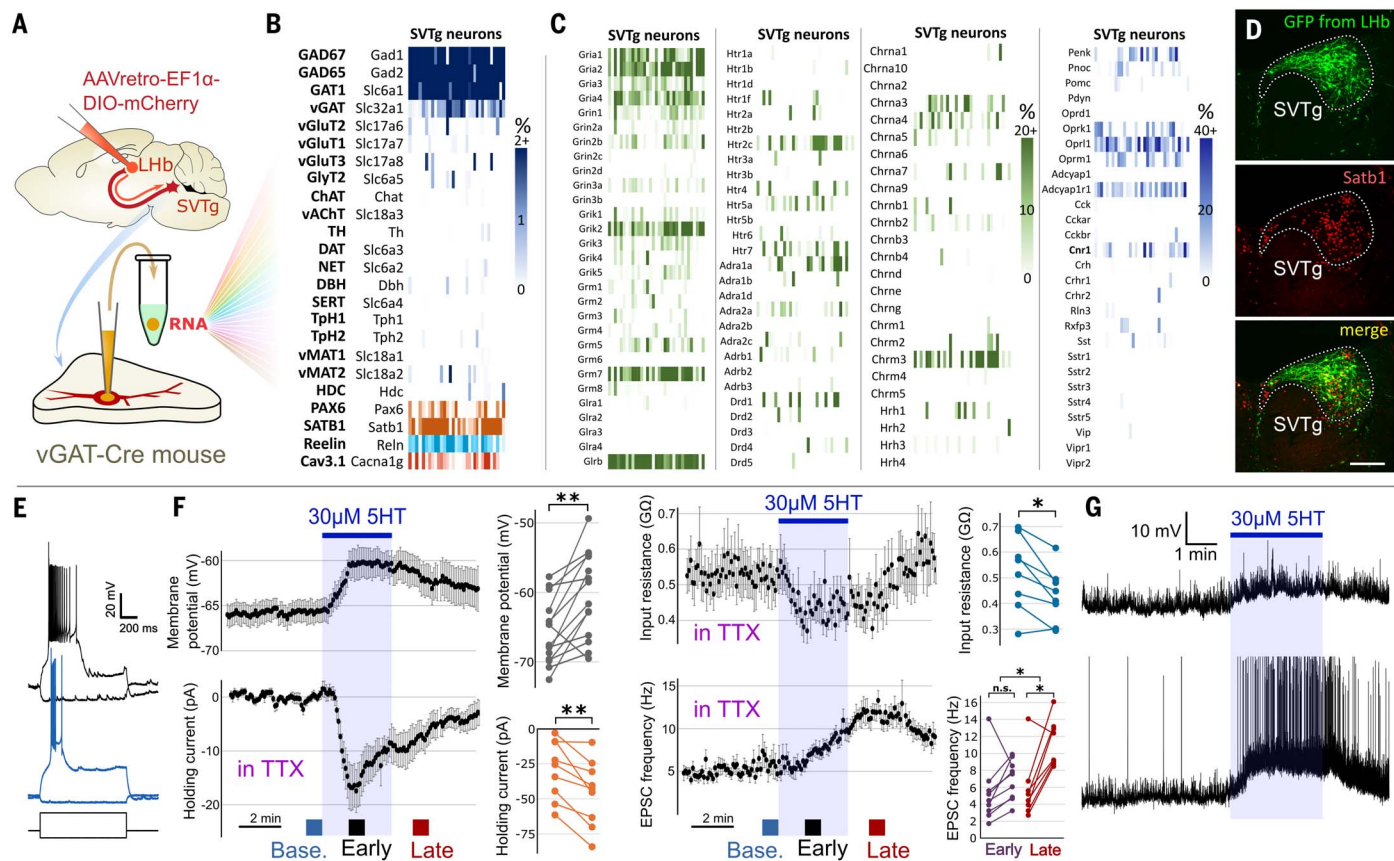


Fig. 7. Gene expression profile and in vitro electrophysiological properties

of SVTg neurons. (A) Cre-dependent mCherry-expressing retrograde AAV was injected into the Lhb of vGAT-Cre mice ($n = 5$) to label SVTg GABAergic neurons. These neurons were tested in electrophysiological experiments and sampled for whole-cell RNA sequencing using Patch-seq analyses. (B) Heatmap represents relative expression (tpm count) of major neurotransmission-related genes (dark blue) and some other typical highly expressed genes (Pax6, Satb1, Reln, Cacna1g) collected from 33 individual SVTg neurons. For more genes and all color scalebars, see fig. S11. (C) Heatmaps represent the relative expression (tpm count) of neurotransmitter receptors (green) as well as neuropeptides and their receptors (blue). (D) Fluorescent images show that retrogradely labeled GFP-containing SVTg neurons (green) are positive for Satb1 (red; for details, see figs. S12 and S13).

Oprml, Fig. 7C and fig. S11, B to H). We found high expression of reelin (Reln), calcium ion channel 1G (Cacna1g) and distinct transcription factor genes (Satb1, Pax6) in SVTg neurons (Fig. 7B and fig. S11, A to H).

Further immunostaining experiments revealed that almost all SVTg neurons express Satb1, Pax6, and Reln at the full rostro-caudal extent of the nucleus (Fig. 7D and figs. S12 and S13). Furthermore, our results suggest that Satb1 is the best candidate to be used as a marker to identify the SVTg in the pons (figs. S12 and S13 and table S12).

Nardone *et al.* recently described the whole transcriptomic profile of the mouse dorsal pontine region (50). Our RNA sequencing suggests that SVTg neurons correspond to the “*Reln/Satb1*” GABAergic neuronal cluster and the

“*II_Reln*” MERFISH cluster in that database, which is located under the fourth ventricle (fig. S14, A to C). The same study (50) confirmed that the SVTg differs from other pontine clusters and that they specifically express not only Satb1, Reln and Pax6 but also Drd1 and several other distinct receptors and ion channel genes (fig. S14, D to E), which may later be used to pharmacologically target SVTg neurons.

The SVTg reward center is strongly activated by serotonin

We next investigated how the neurophysiological and cellular properties of SVTg neurons support their fast and effective control of reward processing. Using in vitro electrophysiological recordings (fig. S15, A and B) we found that all (83 out of 83) SVTg neurons, in the entire

and table S12). Scale bar, 200 μ m. (E) Representative firing properties from two representative SVTg neurons (black and blue traces). Note the burst firing and the spontaneous EPSPs (for details, see fig. S15). (F) Average effect of 30- μ M serotonin (5HT) on membrane potential in control condition (14 SVTg neurons), on holding current (9 SVTg neurons) and input resistance (8 SVTg neurons) in voltage clamp recordings in the presence of 1 μ M TTX, and on the frequency of EPSPs (9 SVTg neurons) in the presence of TTX. As shown in the graphs on the right, 5HT application induced significant changes in these parameters. Effects were measured 70 to 120 s after 5HT application, except for late changes (225 to 275 s) (for more details, see fig. S16). (G) 5HT evoked membrane potential changes in two representative SVTg neurons. Action potentials are truncated for clarity. 5HT elicited spontaneous firing in 2 out of 14 tested SVTg neurons. For statistical details, see table S2.

rostro-caudal and medio-lateral extent of the nucleus, elicited burst firing, further confirming that they belong to the same nucleus (Fig. 7E, and fig. S15, I and M). This burst firing was eliminated by selective blockade of T-type calcium (Cav3) channels (NNC 55-0396; fig. S15, C to E, and table S2), and our immunostaining showed that almost all SVTg neurons expressed Cav3.1 (figs. S12E and S15J), consistent with our mRNA data.

SVTg neurons received large amplitude excitatory postsynaptic events (EPSPs), which completely disappeared in the presence of AMPA-type glutamate receptor inhibitor, NBQX (fig. S15, F to H, and table S2). Our post hoc anatomical investigations revealed that several vGluT1 and vGluT2 terminals surround SVTg neurons (fig. S15K), further suggesting that their activity

is under continuous cortical (vGluT1) and subcortical (vGluT2) glutamatergic control. Our anatomical reconstruction of these *in vitro* recorded SVTg neurons revealed their morphological homogeneity and confirmed that they had an especially long, sparsely spiny dendritic arborization (fig. S17, A to C). All (26 out of 26) tested SVTg neurons expressed Satb1 (fig. S15L), consistent with the mRNA data.

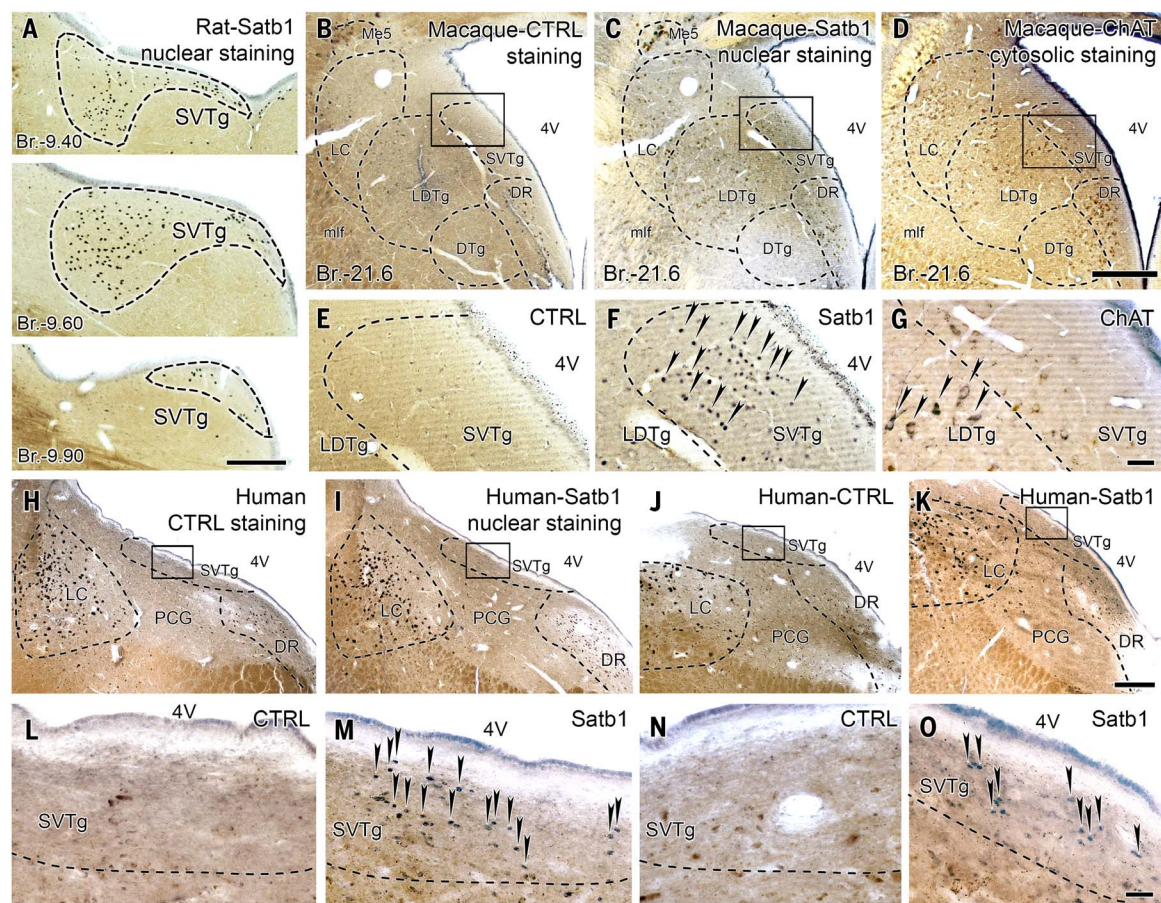
To better understand the links between the anxiolytic effects of SVTg stimulation and the central roles of the serotonergic systems in mood disorders, we next investigated serotonergic signaling in SVTg neurons (51–53). Using *in vitro* slice recordings, we found that serotonin had dual excitatory effects in SVTg neurons. Application of serotonin activated a depolarizing conductance in SVTg cells (Fig. 7, F and G, and table S2) that was independent of synaptic

drive (persistent in the presence of TTX) and was abolished by a selective 5HT7 receptor antagonist (SB269970; fig. S16, A to C, and table S2). On the other hand, serotonin increased the frequency of spontaneous glutamatergic synaptic events in SVTg cells; this effect persisted during 5HT7 receptor blockade, suggesting at least two independent pathways mediate serotonin-induced excitation of SVTg cells. (Fig. 7F, fig. S16, A, D, and E, and table S2). Our anatomical investigations confirmed that SVTg neurons receive innervation from serotonergic axonal fibers (fig. S16F), and that some of these fibers formed classical synaptic contacts (fig. S16G). These *in vitro* recordings also demonstrated that the excitability properties of GABAergic SVTg neurons are homogeneous, as they can easily elicit burst firing and receive strong glutamatergic and serotonergic drive.

The SVTg in rat, macaque, and human brains

The pontine brainstem is thought to be evolutionarily ancient and well conserved, so its neuron populations are likely to be present or even more evolved in most mammalian brains (54). Because Satb1 expression is highly specific for mouse SVTg neurons in the brainstem (Fig. 7D and figs. S12 and S13), we used it to localize the SVTg in the rat, rhesus monkey (*Macaca mulatta*), and human pons. In the rat, we found the Satb1-positive neurons in the same location as in the mouse (Fig. 8A and fig. S18, A and B). In macaque and human brains, noradrenergic LC and serotonergic DR neurons contain neuromelanin, allowing their localization without specific staining (fig. S19F). In three macaque brains (Fig. 7, B to G, and fig. S18, C to N) and in samples from two individuals (Fig. 7, H to O, and fig. S19, A to H), we found Satb1-positive

Fig. 8. Satb1-positive SVTg neurons identified in the rat, monkey, and human dorsal pons. (A) Light microscopic images show Satb1-positive SVTg neurons (black nuclear DAB-Ni staining) in rat pons under the fourth ventricle at three different Bregma coordinates. Scale bar, 200 μm. (B) to (G) Representative images show control staining (no labeling without Satb1 primary antibody) and the localization of Satb1-positive SVTg neurons in rhesus macaque pontine sections (at Bregma –21.6 mm). (B) to (D) Images show the map of pontine nuclei on coronal sections of one side of the dorsal pons. Scale bar, 500 μm. (E) to (G) Images show SVTg areas [indicated with black boxes in (B) to (D)] at higher magnification. Scale bar, 50 μm. (B)



[indicated with black boxes in (H) to (K)]. Scale bar, 50 μm. (H), (J), (L), and (N) Control staining, images show no DAB-Ni labeling without the Satb1 primary antibody. The brown, natively lipofuscin or neuromelanin-expressing cells are detectable (see fig. S19F) in LC and DR without staining. (I), (K), (M), and (O) Satb1 nuclear staining (black DAB-Ni precipitate) reveals a group of neurons (black arrowheads) under the fourth ventricle in a human individual (SKO30). Abbreviations, 4V, fourth ventricle; DR, dorsal raphe; DTg, dorsal tegmentum; LC, locus coeruleus; LDTg, laterodorsal tegmentum; Me5, mesencephalic trigeminal nucleus; mlf, medial longitudinal fasciculus; PCG, pontine central gray; SVTg, subventricular tegmental nucleus.

neurons just below the fourth ventricle (< 300 μm), between LDTg, LC, and DR neurons. Negative and positive controls are also presented (Fig. 7 and figs. S18 and S19).

Discussion

Localization of the SVTg

Previously, specific markers helped in the early recognition of pontine LDTg, LC, and DR, whereas other pontine neurons were identified using viral techniques (23, 55). We discovered the SVTg under the fourth ventricle, as a previously uncharacterized region of the PCG. The GABAergic SVTg is homogenous electrophysiologically (with characteristic firing and serotonin sensitivity), genetically (all expressed a similar set of genes), and anatomically (with identical molecular profiles), whereas its role in modulating behavior in mice is completely different from adjacent GABAergic neurons (48, 56–59).

The evolutionarily ancient LHb, the major target of the SVTg, can be found from cyclostomes to humans (2, 3, 8, 9). Using SVTg-specific Satb1 immunohistochemistry, we identified the SVTg in mice, rats, monkeys, and humans, expanding previous studies reporting Satb1-positive neurons under the fourth ventricle even in bony fishes (60). This suggests that the SVTg is evolutionarily highly conserved.

The SVTg is a major pontine reward center

The SVTg is rapidly activated by both rewarding and reward-predicting stimuli. Direct stimulation of SVTg GABAergic neurons induced a positive motivational state whereas their suppression induced aversion and prevented positive associations. When given a choice, mice self-stimulated their SVTg GABAergic neurons and continued to try repetitively, even after it became impossible, suggesting that these cells may also contribute to reward-seeking and addictive behavior. Our genetic analyses showed that SVTg neurons can process signals from multiple reward-related pathways, including dopaminergic, serotonergic, opioid, and cannabinoid neurotransmitter systems. Moreover, stimulation of SVTg neurons could induce reward-related dopamine release in the NAcc, similar to natural reward stimulus, highlighting that SVTg activity can induce a brain-wide reward experience.

SVTg GABAergic inhibitory neurons massively innervate the negative valence center, the LHb, which constantly optimizes decision-making (3, 15, 16), responds to aversive events and signals their prediction, and encodes the “negative reward prediction error” (2, 5, 13, 61). However, the LHb can also encode rewards by receiving direct inhibitory signals (35–37), making the LHb one of the most important subcortical emotional and valence processing centers (3, 9, 13). However, the inhibition of LHb re-

mained poorly understood (14, 35, 62). We found that the SVTg provides the largest purely inhibitory input to the LHb, shutting down the negative experience mediated by LHb neurons during rewarding events, and thus creating a positive valence. We also found that direct stimulation of SVTg axonal fibers in the LHb was sufficient to induce a positive motivational state in mice.

Besides innervating the LHb, some axon collaterals of the same SVTg GABAergic neurons targeted other brain areas (fig. S21), including other negative emotion-related brain regions such as the lateral hypothalamus (19, 20), lateral preoptic area (21), and median raphe region (23). Some SVTg fibers also targeted the anterior portion of the paraventricular thalamus (PVT), which may contribute to the inhibition of PVT (the origin of which is poorly understood) during unexpected and expected reward experience (63). Furthermore, SVTg axon collaterals also targeted some memory-related brain areas that project to the hippocampus (fig. S21).

The constant activity of the SVTg may play a key role in creating balanced valence and normally motivated behavior, as inhibition of SVTg neurons suppressed spatial exploration and caused place avoidance. The activity of SVTg neurons can be controlled and upregulated by the abundant glutamatergic prefrontal neocortical inputs, including those from the OFC, which can modulate valence processing, motivation, and decision-making based on experience (64–66).

We found that the SVTg continuously balances the valence circuitry as well during negative experiences. Aversive stimuli rapidly activated SVTg GABAergic neurons, probably to prevent overexcitation of the LHb (18, 62, 67). Indeed, the suppression of SVTg GABAergic neurons during aversive experiences produced abnormally strong fear memories, whereas their overactivation during aversive experiences prevented the formation of normal fear responses. However, SVTg neuronal activity also showed adaptations on a behavioral timescale during a series of negative events. This adaptation can downscale the inhibition of LHb in continuously aversive more threatening situations. This suggests that the SVTg keeps LHb signaling under control as a function of external stimuli to prevent the development of an excessive fear response and to prevent the formation of abnormal overgeneralization. Therefore, the SVTg may also play a role in decision-making (3, 15, 16).

Regulation of the reward processing in the SVTg

The fast and powerful reward control of the SVTg requires effective fine-tuning that may originate from brain areas that process salient environmental stimuli (PRN, mRT, Gi), negative experiences (MRR, IPN, LHb, LH) (17, 20, 23, 49),

positive experiences (OFC, LDTg, DR, VTA) (4, 59, 66, 68) and decision-making (ACC, ZI, SC, SNr; fig. S21). Our mRNA sequencing also revealed that the SVTg can process various neuromodulatory signals involved in reward processing.

The evolutionarily ancient pontine nuclei have had ample time to coevolve and fine-tune their connections with associative cortical areas as well (54, 69). We found that pyramidal cells from various higher-order neocortical centers, including the anterior cingulate cortex, medial prefrontal cortex (mPFC), and especially the OFC, converge onto SVTg neurons (fig. S21). The function of OFC in processing reward prediction, reward expectation, and motivation is well-established (64–66). However, the mechanism by which the OFC executes this function is not fully understood. We found that OFC abundantly targets SVTg neurons. Stimulation of their terminals in the SVTg induced a positive experience and reduced the strength of fear memory formation in mice, similar to the direct stimulation of SVTg neurons. This OFC connection can therefore be critically important for valence encoding to control reward prediction through the OFC-SVTg-LHb axis (fig. S21).

Potential clinical relevance

The reward-related activity of the SVTg and our findings that mice self-stimulated their own SVTg, whereas this stimulation induced dopamine release in the NAcc, suggest that the SVTg may play a role in addiction. This is supported by the expression of several types of receptors associated with addiction in SVTg neurons.

Hyperactivation of LHb neurons is known to play a central role in anxiety and major depressive disorders in humans and their rodent models (9–11, 27, 28, 30, 32) and recent therapeutic approaches aim to suppress LHb activity (with ketamine or clinical deep brain stimulation) (27, 29, 38, 39). We found that the SVTg can effectively inhibit LHb and reduce anxiety in mice. Therefore, suppressed SVTg activity may contribute to these disorders, whereas clinical activation of the SVTg may have therapeutic effects.

Because serotonin—the neurotransmitter system frequently targeted in the treatment of depression (51–53)—can robustly excite SVTg neurons, selective serotonin reuptake inhibitors may affect the SVTg→LHb pathway. Other mood-altering compounds (for instance, LSD) (70, 71) may also act on serotonin receptors of the SVTg.

The early stages of Alzheimer’s and Parkinson’s diseases are manifested in the pontine brainstem (72–74). Therefore, one may speculate that the SVTg may contribute to the development of emotional dysfunction in these diseases. Understanding the vulnerability of the SVTg in these

processes may help to better understand these disorders.

Materials and methods summary

Ethical considerations, mouse strains, rats, monkey, and human samples

Experiments were conducted in accordance with Hungarian animal research regulations and EU Directive 2010/63/EU, with approval from relevant ethical bodies. Various mouse strains (vGAT-Cre, vGluT1-Cre, vGluT2-Cre, ChAT-Cre, SOM-Cre, vGAT-Flp, and vGAT/ZsGreen) were used for experiments, along with adult male Wistar rats, rhesus macaque monkeys, and human brainstem samples. The rats and monkeys were previously studied, and their stored brainstem samples were reanalyzed. The human samples were obtained postmortem with informed consent, following ethical guidelines and the Declaration of Helsinki. For details, see the complete materials and methods in the supplementary materials.

Viral gene transfer, retrograde and mono-transsynaptic rabies tracing, and optic fiber implantations

Mice were anesthetized and mounted in an animal stereotaxic frame. A microinjector pump was used for injections. For anterograde and retrograde tracing, optogenetic behavioral experiments, fiber photometry, and *in vivo* and *in vitro* electrophysiology experiments, we injected different amounts of retrogradely or anterogradely transmitted viruses into the target brain areas. All used viral constructs are presented in table S7 and all brain coordinates used are listed in table S8. For behavioral experiments, optic fibers were implanted over the target brain areas 4 to 6 weeks after virus injections. Virus injection sites and the positions of the optic fibers are illustrated in fig. S20. For rabies tracing experiment mice were injected with a Cre-dependent helper AAV into the SVTg, followed by a rabies virus into the LHb, and after immunohistochemistry, rabies-labeled brain areas were visualized and analyzed. For details, see the complete materials and methods in the supplementary materials.

Perfusions

Mice were anesthetized and perfused transcardially with paraformaldehyde-containing solution. After perfusions, brains were cut into 50-, 60-, or 100- μm -thick sections using a vibratome. For details, see the complete materials and methods in the supplementary materials.

Immunohistochemistry, antibodies, and cell counting

Generally, perfusion-fixed sections were cryoprotected, and after antigen retrieval they were incubated in a blocking solution, and sections were incubated in a mixture of primary antibodies. This was followed by extensive washes

and incubation in the mixture of appropriate secondary antibodies. Then, sections were placed on slides and covered with mounting medium. Fluorescent immunohistochemistry for epifluorescent microscopy, laser-scanning confocal microscopy, immunogold-immunoperoxidase double labeling for electron microscopy required different procedures, which are described in detail in the supplementary methods. The list and specifications of the primary and secondary antibodies used in the study can be found in tables S9 and S10. Combinations of the used primary and secondary antibodies in the different experiments are listed in table S11. After imaging of the sections, cell counting was performed using NIS-Elements AR 4.3 or NIS-Elements 5.3 or Adobe Photoshop CS6 Extended software. For details, see the complete materials and methods in the supplementary materials.

Immunoperoxidase experiment for rat, monkey, and human samples

Perfusion-fixed rat, macaque, and human brains were embedded in agarose, sectioned, and processed for antigen retrieval and immunohistochemistry. After blocking and extensive washes, sections were incubated with or without (CTRL staining) primary antibodies, followed by secondary antibody staining and development using DAB-Ni. The sections were then contrasted, dehydrated, embedded in Durcupan, and imaged using a brightfield microscope. For details, see the complete materials and methods in the supplementary materials.

In vivo electrophysiological recording experiment

Surgical procedures involved attaching a headplate to mice under anesthesia and drilling cranial windows for electrode and optical fiber placement. After recovery, *in vivo* electrophysiological recordings were performed with a 128-channel silicon probe in the LHb and an optical fiber in the SVTg, while the mice were free to move on a floating ball. Neuronal activity was recorded while mice received laser stimulations or air puffs, and these data were analyzed with spike sorting performed using specialized software. For details, see the complete materials and methods in the supplementary materials.

Optogenetic behavior experiments

After optic fiber implantations, mice were transferred to the animal room of the behavioral unit of the institute to rest, followed by 5 days of handling. We carried out real-time place-preference or aversion tests (RTPP/RTPA), conditioned place-preference or aversion tests (CPP/CPA), pellet-induced place preference test, elevated plus maze test (EPM), operant self-stimulation tests, and contextual fear conditioning tests. Experimental data were collected or analyzed using the Noldus EthoVision and TIBCO Statistica software. Freezing behavior of mice was recorded and analyzed with a custom-made freezing de-

tection head-mounted sensor. For details, see the complete materials and methods in the supplementary materials.

Fiber photometry experiments

After 400- μm -thick optic fiber implantation, mice were transferred to the animal room of the behavioral unit of the institute to rest and then received five days of handling. We carried out head-fixed fiber photometry experiments, where neural activity was recorded in awake mice using a Doric-based, custom-built setup. Mice underwent various behavioral tests, including unpredicted water and sucrose rewards, tone-predicted rewards, neutral light, and tone cues, and aversive air puffs and air puff trains. Fluorescent signals from GCaMP8m expressed in SVTg neurons were collected from both activity-dependent (465 nm) and control isosbestic (405 nm) signals were recorded simultaneously. Fluorescent signals from DA4.4 expressed in NAcc neurons were collected from mice during SVTg optogenetic activation and water rewards. Data processing involved using the isosbestic signal to correct for motion artifacts and photo-bleaching, calculating $\Delta F/F$ signals, which were then analyzed and normalized using z-scores to account for variability across sessions and subjects. For details, see the complete materials and methods in the supplementary materials.

In vitro electrophysiology and single cell mRNA collection

In vitro electrophysiology experiments were conducted on 200- to 250- μm -thick brainstem slices containing the virally labeled SVTg. Neurons were visualized, patched, and recorded to measure basic electrophysiological properties, and simultaneously exposed to various types of drugs (NNC 55-0396, NBQX, TTX, 5HT, SB269970). Data processing included analyzing EPSP frequency and amplitude, with pharmacological experiments conducted using various amplifiers and software. Some recorded cells were also reconstructed in 3D using the Neurolucida System. For details, see the complete materials and methods in the supplementary materials.

Single-cell mRNA sequencing and analysis

After electrophysiological recordings, single-cell mRNA was collected from SVTg cells by aspirating the cytosol into microtubes, then frozen and stored for processing. mRNA was reverse transcribed to cDNA, amplified, and prepared for sequencing using the SMART-Seq HT PLUS Kit. Sequencing was performed on a NovaSeq 6000, and the data were processed by aligning reads to the mm39 reference genome. Low-quality cells were excluded, and gene expression profiles of each cell were visualized using heatmaps based on the percentage of tpm counts. For details, see the complete materials and methods in the supplementary materials.

Statistical analysis

For non-Gaussian data, we used median and interquartile range for presentation. We used Mann–Whitney U-tests, Wilcoxon signed-rank tests, and *t*-tests for statistical analysis, with significance levels indicated as, n.s. ($P > 0.05$), *($P < 0.05$), **($P < 0.01$), ***($P < 0.001$), and ****($P < 0.0001$). All statistical details and *P*-values are presented in tables S2 to S4. For details, see the complete materials and methods in the supplementary materials.

REFERENCES AND NOTES

- K. C. Berridge, Affective valence in the brain, Modules or modes? *Nat. Rev. Neurosci.* **20**, 225–234 (2019). doi: [10.1038/s41583-019-0122-8](https://doi.org/10.1038/s41583-019-0122-8); pmid: [30718826](https://pubmed.ncbi.nlm.nih.gov/30718826/)
- H. Hu, Reward and Aversion. *Annu. Rev. Neurosci.* **39**, 297–324 (2018). doi: [10.1146/annurev-neuro-070815-014106](https://doi.org/10.1146/annurev-neuro-070815-014106); pmid: [27145915](https://pubmed.ncbi.nlm.nih.gov/27145915/)
- O. Hikosaka, The habenula: From stress evasion to value-based decision-making. *Nat. Rev. Neurosci.* **11**, 503–513 (2010). doi: [10.1038/nrn2866](https://doi.org/10.1038/nrn2866); pmid: [20559337](https://pubmed.ncbi.nlm.nih.gov/20559337/)
- S. Lammel et al., Input-specific control of reward and aversion in the ventral tegmental area. *Nature* **491**, 212–217 (2012). doi: [10.1038/nature11527](https://doi.org/10.1038/nature11527); pmid: [23064228](https://pubmed.ncbi.nlm.nih.gov/23064228/)
- M. Matsumoto, O. Hikosaka, Lateral habenula as a source of negative reward signals in dopamine neurons. *Nature* **447**, 1111–1115 (2007). doi: [10.1038/nature05860](https://doi.org/10.1038/nature05860); pmid: [17522629](https://pubmed.ncbi.nlm.nih.gov/17522629/)
- M. Matsumoto, O. Hikosaka, Two types of dopamine neuron distinctly convey positive and negative motivational signals. *Nature* **459**, 837–841 (2009). doi: [10.1038/nature08028](https://doi.org/10.1038/nature08028); pmid: [19448610](https://pubmed.ncbi.nlm.nih.gov/19448610/)
- C. Xiao et al., Glutamatergic and GABAergic neurons in pontine central gray mediate opposing valence-specific behaviors through a global network. *Neuron* **111**, 1486–1503.e7 (2023). doi: [10.1016/j.neuron.2023.02.012](https://doi.org/10.1016/j.neuron.2023.02.012); pmid: [36893756](https://pubmed.ncbi.nlm.nih.gov/36893756/)
- M. Stephenson-Jones, O. Floros, B. Robertson, S. Grillner, Evolutionary conservation of the habenular nuclei and their circuitry controlling the dopamine and 5-hydroxytryptophan (5-HT) systems. *Proc. Natl. Acad. Sci. U.S.A.* **109**, E164–E173 (2012). doi: [10.1073/pnas.1119348109](https://doi.org/10.1073/pnas.1119348109); pmid: [22203996](https://pubmed.ncbi.nlm.nih.gov/22203996/)
- H. Hu, Y. Cui, Y. Yang, Circuits and functions of the lateral habenula in health and in disease. *Nat. Rev. Neurosci.* **21**, 277–295 (2020). doi: [10.1038/s41583-020-0292-4](https://doi.org/10.1038/s41583-020-0292-4); pmid: [32269316](https://pubmed.ncbi.nlm.nih.gov/32269316/)
- H. Aizawa, W. Cui, K. Tanaka, H. Okamoto, Hyperactivation of the habenula as a link between depression and sleep disturbance. *Front. Hum. Neurosci.* **7**, 826 (2013). doi: [10.3389/fnhum.2013.00826](https://doi.org/10.3389/fnhum.2013.00826); pmid: [24339810](https://pubmed.ncbi.nlm.nih.gov/24339810/)
- K. Ranft et al., Evidence for structural abnormalities of the human habenular complex in affective disorders but not in schizophrenia. *Psychol. Med.* **40**, 557–567 (2010). doi: [10.1017/S0033291709990821](https://doi.org/10.1017/S0033291709990821); pmid: [1967211](https://pubmed.ncbi.nlm.nih.gov/1967211/)
- M. Stephenson-Jones et al., A basal ganglia circuit for evaluating action outcomes. *Nature* **539**, 289–293 (2016). doi: [10.1038/nature18845](https://doi.org/10.1038/nature18845); pmid: [27652894](https://pubmed.ncbi.nlm.nih.gov/27652894/)
- C. D. Proulx, O. Hikosaka, R. Malinow, Reward processing by the lateral habenula in normal and depressive behaviors. *Nat. Neurosci.* **17**, 1146–1152 (2014). doi: [10.1038/nn.3779](https://doi.org/10.1038/nn.3779); pmid: [25157511](https://pubmed.ncbi.nlm.nih.gov/25157511/)
- H. Li, D. Pullmann, T. C. Jhou, Valence-encoding in the lateral habenula arises from the entopeduncular region. *eLife* **8**, 1–17 (2019). doi: [10.7554/eLife.41223](https://doi.org/10.7554/eLife.41223); pmid: [30855228](https://pubmed.ncbi.nlm.nih.gov/30855228/)
- C. M. Stopper, M. T. L. Tse, D. R. Montes, C. R. Wiedman, S. B. Floresco, Overriding phasic dopamine signals redirects action selection during risk/reward decision making. *Neuron* **84**, 177–189 (2014). doi: [10.1016/j.neuron.2014.08.033](https://doi.org/10.1016/j.neuron.2014.08.033); pmid: [25220811](https://pubmed.ncbi.nlm.nih.gov/25220811/)
- C. M. Stopper, S. B. Floresco, What's better for me? Fundamental role for lateral habenula in promoting subjective decision biases. *Nat. Neurosci.* **17**, 33–35 (2014). doi: [10.1038/nn.3587](https://doi.org/10.1038/nn.3587); pmid: [24270185](https://pubmed.ncbi.nlm.nih.gov/24270185/)
- A. M. Stamatakis, G. D. Stubber, Activation of lateral habenula inputs to the ventral midbrain promotes behavioral avoidance. *Nat. Neurosci.* **15**, 1105–1107 (2012). doi: [10.1038/nn.3145](https://doi.org/10.1038/nn.3145); pmid: [22729176](https://pubmed.ncbi.nlm.nih.gov/22729176/)
- T. E. Sachella et al., A novel role for the lateral habenula in fear learning. *Neuropsychopharmacology* **47**, 1210–1219 (2022). doi: [10.1038/s41386-022-01294-5](https://doi.org/10.1038/s41386-022-01294-5); pmid: [35217797](https://pubmed.ncbi.nlm.nih.gov/35217797/)
- I. Lazaridis et al., A hypothalamus-habenula circuit controls aversion. *Mol. Psychiatry* **24**, 1351–1368 (2019). doi: [10.1038/s41380-019-0369-5](https://doi.org/10.1038/s41380-019-0369-5); pmid: [30755721](https://pubmed.ncbi.nlm.nih.gov/30755721/)
- D. Calvignoni et al., Esr1⁺ hypothalamic-habenula neurons shape aversive states. *Nat. Neurosci.* **26**, 1245–1255 (2023). doi: [10.1038/s41593-023-01367-8](https://doi.org/10.1038/s41593-023-01367-8); pmid: [37349481](https://pubmed.ncbi.nlm.nih.gov/37349481/)
- D. J. Barker et al., Lateral Preoptic Control of the Lateral Habenula through Convergent Glutamate and GABA Transmission. *Cell Rep.* **21**, 1757–1769 (2017). doi: [10.1016/j.celrep.2017.10.066](https://doi.org/10.1016/j.celrep.2017.10.066); pmid: [29141211](https://pubmed.ncbi.nlm.nih.gov/29141211/)
- J. H. Yoo et al., Ventral tegmental area glutamate neurons co-release GABA and promote positive reinforcement. *Nat. Commun.* **7**, 13697 (2016). doi: [10.1038/ncomms13697](https://doi.org/10.1038/ncomms13697); pmid: [27976722](https://pubmed.ncbi.nlm.nih.gov/27976722/)
- A. Szönyi et al., Median raphe controls acquisition of negative experience in the mouse. *Science* **366**, eaay8746 (2019). doi: [10.1126/science.aaay8746](https://doi.org/10.1126/science.aaay8746); pmid: [31780530](https://pubmed.ncbi.nlm.nih.gov/31780530/)
- G.-W. Zhang et al., Transforming Sensory Cues into Aversive Emotion via Septal-Habenular Pathway. *Neuron* **99**, 1016–1028.e5 (2018). doi: [10.1016/j.neuron.2018.07.023](https://doi.org/10.1016/j.neuron.2018.07.023); pmid: [30122379](https://pubmed.ncbi.nlm.nih.gov/30122379/)
- Y. Cui et al., Reward ameliorates depressive-like behaviors via inhibition of the substantia innominata to the lateral habenula projection. *Sci. Adv.* **8**, eabn0193 (2022). doi: [10.1126/sciadv.abn0193](https://doi.org/10.1126/sciadv.abn0193); pmid: [35857453](https://pubmed.ncbi.nlm.nih.gov/35857453/)
- S. J. Shabel, C. D. Proulx, A. Trias, R. T. Murphy, R. Malinow, Input to the lateral habenula from the basal ganglia is excitatory, aversive, and suppressed by serotonin. *Neuron* **74**, 475–481 (2012). doi: [10.1016/j.neuron.2012.02.037](https://doi.org/10.1016/j.neuron.2012.02.037); pmid: [22578499](https://pubmed.ncbi.nlm.nih.gov/22578499/)
- Y. Yang et al., Ketamine blocks bursting in the lateral habenula to rapidly relieve depression. *Nature* **554**, 317–322 (2018). doi: [10.1038/nature25509](https://doi.org/10.1038/nature25509); pmid: [29446381](https://pubmed.ncbi.nlm.nih.gov/29446381/)
- Y. Cui et al., Astroglial Kir4.1 in the lateral habenula drives neuronal bursts in depression. *Nature* **554**, 323–327 (2018). doi: [10.1038/nature25752](https://doi.org/10.1038/nature25752); pmid: [29446379](https://pubmed.ncbi.nlm.nih.gov/29446379/)
- S. Ma et al., Sustained antidepressant effect of ketamine through NMDAR trapping in the LHb. *Nature* **622**, 802–809 (2023). doi: [10.1038/s41586-023-06624-1](https://doi.org/10.1038/s41586-023-06624-1); pmid: [37853123](https://pubmed.ncbi.nlm.nih.gov/37853123/)
- B. Li et al., Synaptic potentiation onto habenula neurons in the learned helplessness model of depression. *Nature* **470**, 535–539 (2011). doi: [10.1038/nature09742](https://doi.org/10.1038/nature09742); pmid: [21350486](https://pubmed.ncbi.nlm.nih.gov/21350486/)
- K. Li et al., pCaMKII in lateral habenula mediates core symptoms of depression. *Science* **341**, 1016–1020 (2013). doi: [10.1126/science.1240729](https://doi.org/10.1126/science.1240729); pmid: [23990563](https://pubmed.ncbi.nlm.nih.gov/23990563/)
- S. J. Shabel, C. Wang, B. Monk, S. Aronson, R. Malinow, Stress transforms lateral habenula reward responses into punishment signals. *Proc. Natl. Acad. Sci. U.S.A.* **116**, 12488–12493 (2019). doi: [10.1073/pnas.1903334116](https://doi.org/10.1073/pnas.1903334116); pmid: [3152135](https://pubmed.ncbi.nlm.nih.gov/3152135/)
- A. Nuno-Perez et al., Stress undermines reward-guided cognitive performance through synaptic depression in the lateral habenula. *Neuron* **109**, 947–956.e5 (2021). doi: [10.1016/j.neuron.2021.01.008](https://doi.org/10.1016/j.neuron.2021.01.008); pmid: [33535028](https://pubmed.ncbi.nlm.nih.gov/33535028/)
- D. Knowland et al., Distinct Ventral Pallidal Neural Populations Mediate Separate Symptoms of Depression. *Cell* **170**, 284–297.e18 (2017). doi: [10.1016/j.cell.2017.06.015](https://doi.org/10.1016/j.cell.2017.06.015); pmid: [28689640](https://pubmed.ncbi.nlm.nih.gov/28689640/)
- A. L. Lalive et al., Synaptic inhibition in the lateral habenula shapes reward anticipation. *Curr. Biol.* **32**, 1829–1836.e4 (2022). doi: [10.1016/j.cub.2022.02.035](https://doi.org/10.1016/j.cub.2022.02.035); pmid: [35259343](https://pubmed.ncbi.nlm.nih.gov/35259343/)
- D. Wang et al., Learning shapes the aversion and reward responses of lateral habenula neurons. *eLife* **6**, 1–20 (2017). doi: [10.7554/eLife.23045](https://doi.org/10.7554/eLife.23045); pmid: [28561735](https://pubmed.ncbi.nlm.nih.gov/28561735/)
- L. Shen et al., A bottom-up reward pathway mediated by somatostatin neurons in the medial septal complex underlying appetitive learning. *Nat. Commun.* **13**, 1194 (2022). doi: [10.1038/s41467-022-28854-z](https://doi.org/10.1038/s41467-022-28854-z); pmid: [35256596](https://pubmed.ncbi.nlm.nih.gov/35256596/)
- A. Sartorius et al., Remission of major depression under deep brain stimulation of the lateral habenula in a therapy-refractory patient. *Biol. Psychiatry* **67**, e9–e11 (2010). doi: [10.1016/j.biopsych.2009.08.027](https://doi.org/10.1016/j.biopsych.2009.08.027); pmid: [19846068](https://pubmed.ncbi.nlm.nih.gov/19846068/)
- C. Zhang et al., Habenula deep brain stimulation for refractory bipolar disorder. *Brain Stimul.* **12**, 1298–1300 (2019). doi: [10.1016/j.brs.2019.05.010](https://doi.org/10.1016/j.brs.2019.05.010); pmid: [31103455](https://pubmed.ncbi.nlm.nih.gov/31103455/)
- F. J. Meye et al., Shifted pallidal co-release of GABA and glutamate in habenula drives cocaine withdrawal and relapse. *Nat. Neurosci.* **19**, 1019–1024 (2016). doi: [10.1038/nn.4334](https://doi.org/10.1038/nn.4334); pmid: [27348214](https://pubmed.ncbi.nlm.nih.gov/27348214/)
- D. H. Root et al., Selective Brain Distribution and Distinctive Synaptic Architecture of Dual Glutamatergic-GABAergic Neurons. *Cell Rep.* **23**, 3465–3479 (2018). doi: [10.1016/j.celrep.2018.05.063](https://doi.org/10.1016/j.celrep.2018.05.063); pmid: [29924991](https://pubmed.ncbi.nlm.nih.gov/29924991/)
- X. Liu, H. Huang, Y. Zhang, L. Wang, F. Wang, Sexual Dimorphism of Inputs to the Lateral Habenula in Mice. *Neurosci. Bull.* **38**, 1439–1456 (2022). doi: [10.1007/s12264-022-00885-y](https://doi.org/10.1007/s12264-022-00885-y); pmid: [35644002](https://pubmed.ncbi.nlm.nih.gov/35644002/)
- T. Patriarchi et al., Ultrafast neuronal imaging of dopamine dynamics with designed genetically encoded sensors. *Science* **360**, eaat4422 (2018). doi: [10.1126/science.aat4422](https://doi.org/10.1126/science.aat4422); pmid: [29853555](https://pubmed.ncbi.nlm.nih.gov/29853555/)
- S. Lammel, B. K. Lim, R. C. Malenka, Reward and aversion in a heterogeneous midbrain dopamine system. *Neuropharmacology* **76**, 351–359 (2014). doi: [10.1016/j.neuropharm.2013.03.019](https://doi.org/10.1016/j.neuropharm.2013.03.019); pmid: [23578393](https://pubmed.ncbi.nlm.nih.gov/23578393/)
- S. R. Sesack, A. A. Grace, Cortico-Basal Ganglia reward network. Microcircuitry. *Neuropsychopharmacology* **35**, 27–47 (2010). doi: [10.1038/npp.2009.93](https://doi.org/10.1038/npp.2009.93); pmid: [19675534](https://pubmed.ncbi.nlm.nih.gov/19675534/)
- H. Kawai et al., Median raphe serotonergic neurons projecting to the interpeduncular nucleus control preference and aversion. *Nat. Commun.* **13**, 7708 (2022). doi: [10.1038/s41467-022-35346-7](https://doi.org/10.1038/s41467-022-35346-7); pmid: [36550097](https://pubmed.ncbi.nlm.nih.gov/36550097/)
- K. E. Sos et al., Cellular architecture and transmitter phenotypes of neurons of the mouse median raphe region. *Brain Struct. Funct.* **222**, 287–299 (2017). doi: [10.1007/s00429-016-1217-x](https://doi.org/10.1007/s00429-016-1217-x); pmid: [27044051](https://pubmed.ncbi.nlm.nih.gov/27044051/)
- C. Liu et al., An inhibitory brainstem input to dopamine neurons encodes nicotine aversion. *Neuron* **110**, 3018–3035.e7 (2022). doi: [10.1016/j.neuron.2022.07.003](https://doi.org/10.1016/j.neuron.2022.07.003); pmid: [35921846](https://pubmed.ncbi.nlm.nih.gov/35921846/)
- S. L. Wolfman et al., Nicotine aversion is mediated by GABAergic interpeduncular nucleus inputs to laterodorsal tegmentum. *Nat. Commun.* **9**, 2710 (2018). doi: [10.1038/s41467-018-04654-2](https://doi.org/10.1038/s41467-018-04654-2); pmid: [30006624](https://pubmed.ncbi.nlm.nih.gov/30006624/)
- S. Nardone et al., A spatially-resolved transcriptional atlas of the murine dorsal pons at single-cell resolution. *Nat. Commun.* **15**, 1966 (2024). doi: [10.1038/s41467-024-45907-7](https://doi.org/10.1038/s41467-024-45907-7); pmid: [38438345](https://pubmed.ncbi.nlm.nih.gov/38438345/)
- A. Rossi, A. Barraco, P. Donda, Fluoxetine, A review on evidence based medicine. *Ann. Gen. Hosp. Psychiatry* **3**, 2 (2004). doi: [10.1186/1475-2832-3-2](https://doi.org/10.1186/1475-2832-3-2); pmid: [14962351](https://pubmed.ncbi.nlm.nih.gov/14962351/)
- F. López-Muñoz, C. Alamo, Monoaminergic neurotransmission, the history of the discovery of antidepressants from 1950s until today. *Curr. Pharm. Des.* **15**, 1563–1586 (2009). doi: [10.2174/13816120978168001](https://doi.org/10.2174/13816120978168001); pmid: [1942174](https://pubmed.ncbi.nlm.nih.gov/1942174/)
- M. Berger, J. A. Gray, B. L. Roth, the expanded biology of serotonin. *Annu. Rev. Med.* **60**, 355–366 (2009). doi: [10.1146/annurev.med.60.042307.110802](https://doi.org/10.1146/annurev.med.60.042307.110802); pmid: [19630576](https://pubmed.ncbi.nlm.nih.gov/19630576/)
- A. Venkatraman, B. L. Edlow, M. H. Immordino-Yang, the Brainstem in Emotion, A Review. *Front. Neuroanat.* **11**, 15 (2017). doi: [10.3389/fnana.2017.00015](https://doi.org/10.3389/fnana.2017.00015); pmid: [28337130](https://pubmed.ncbi.nlm.nih.gov/28337130/)
- A. Szönyi et al., Brainstem nucleus incertus controls contextual memory formation. *Science* **364**, eaaw0445 (2019). doi: [10.1126/science.aaw0445](https://doi.org/10.1126/science.aaw0445); pmid: [31123108](https://pubmed.ncbi.nlm.nih.gov/31123108/)
- L. Brousset et al., A non-canonical GABAergic pathway to the VTA promotes unconditioned freezing. *Mol. Psychiatry* **27**, 4905–4917 (2022). doi: [10.1038/s41380-022-01765-7](https://doi.org/10.1038/s41380-022-01765-7); pmid: [36127430](https://pubmed.ncbi.nlm.nih.gov/36127430/)
- Y. Du et al., Dopamine release and negative valence gated by inhibitory neurons in the laterodorsal tegmental nucleus. *Neuron* **111**, 3102–3118.e7 (2023). doi: [10.1016/j.neuron.2023.06.021](https://doi.org/10.1016/j.neuron.2023.06.021); pmid: [37499661](https://pubmed.ncbi.nlm.nih.gov/37499661/)
- H. Yang et al., Laterodorsal tegmentum interneuron subtypes oppositely regulate olfactory cue-induced innate fear. *Nat. Neurosci.* **19**, 283–289 (2016). doi: [10.1038/nn.4208](https://doi.org/10.1038/nn.4208); pmid: [26727549](https://pubmed.ncbi.nlm.nih.gov/26727549/)
- B. Coimbra et al., Role of laterodorsal tegmentum projections to nucleus accumbens in reward-related behaviors. *Nat. Commun.* **10**, 4138 (2019). doi: [10.1038/s41467-019-11557-3](https://doi.org/10.1038/s41467-019-11557-3); pmid: [31515512](https://pubmed.ncbi.nlm.nih.gov/31515512/)
- D. Lozano et al., Expression of SATB1 and SATB2 in the brain of bony fishes, What fish reveal about evolution. *Brain Struct. Funct.* **228**, 921–945 (2023). doi: [10.1007/s00429-023-02632-z](https://doi.org/10.1007/s00429-023-02632-z); pmid: [37002478](https://pubmed.ncbi.nlm.nih.gov/37002478/)
- M. Matsumoto, O. Hikosaka, Representation of negative motivational value in the primate lateral habenula. *Nat. Neurosci.* **12**, 77–84 (2009). doi: [10.1038/nn.2233](https://doi.org/10.1038/nn.2233); pmid: [19043410](https://pubmed.ncbi.nlm.nih.gov/19043410/)
- M. Congiu et al., Plasticity of neuronal dynamics in the lateral habenula for cue-punishment associative learning. *Mol. Psychiatry* **28**, 518–527 (2023). doi: [10.1038/s41380-023-02155-3](https://doi.org/10.1038/s41380-023-02155-3); pmid: [37414924](https://pubmed.ncbi.nlm.nih.gov/37414924/)
- J. M. Otis et al., Paraventricular Thalamus Projection Neurons Integrate Cortical and Hypothalamic Signals for Cue-Reward Processing. *Neuron* **103**, 423–431.e4 (2019). doi: [10.1016/j.neuron.2019.05.018](https://doi.org/10.1016/j.neuron.2019.05.018); pmid: [31196673](https://pubmed.ncbi.nlm.nih.gov/31196673/)
- V. Pascoli et al., Stochastic synaptic plasticity underlying compulsion in a model of addiction. *Nature* **564**, 366–371 (2018). doi: [10.1038/s41586-018-0789-4](https://doi.org/10.1038/s41586-018-0789-4); pmid: [30568192](https://pubmed.ncbi.nlm.nih.gov/30568192/)
- A. Izquierdo, Functional heterogeneity within rat orbitofrontal cortex in reward learning and decision making. *J. Neurosci.* **37**, 10529–10540 (2017). doi: [10.1523/JNEUROSCI.1678-17.2017](https://doi.org/10.1523/JNEUROSCI.1678-17.2017); pmid: [29093055](https://pubmed.ncbi.nlm.nih.gov/29093055/)

66. V. M. K. Namboodiri *et al.*, Single-cell activity tracking reveals that orbitofrontal neurons acquire and maintain a long-term memory to guide behavioral adaptation. *Nat. Neurosci.* **22**, 1110–1121 (2019). doi: [10.1038/s41593-019-0408-1](https://doi.org/10.1038/s41593-019-0408-1); pmid: [31160741](https://pubmed.ncbi.nlm.nih.gov/31160741/)
67. M. Congiu, M. Trusel, M. Pistic, M. Mameli, S. Lecca, Opposite responses to aversive stimuli in lateral habenula neurons. *Eur. J. Neurosci.* **50**, 2921–2930 (2019). doi: [10.1111/ejn.14400](https://doi.org/10.1111/ejn.14400); pmid: [30860301](https://pubmed.ncbi.nlm.nih.gov/30860301/)
68. J. Qi *et al.*, A glutamatergic reward input from the dorsal raphe to ventral tegmental area dopamine neurons. *Nat. Commun.* **5**, 5390 (2014). doi: [10.1038/ncomms6390](https://doi.org/10.1038/ncomms6390); pmid: [25388237](https://pubmed.ncbi.nlm.nih.gov/25388237/)
69. D. Hain *et al.*, Molecular diversity and evolution of neuron types in the amniote brain. *Science* **377**, eabp8202 (2022). doi: [10.1126/science.abp8202](https://doi.org/10.1126/science.abp8202); pmid: [36048944](https://pubmed.ncbi.nlm.nih.gov/36048944/)
70. J. Glazer, C. H. Murray, R. Nusslock, R. Lee, H. de Wit, Low doses of lysergic acid diethylamide (LSD) increase reward-related brain activity. *Neuropharmacology* **48**, 418–426 (2023). doi: [10.1038/s41386-022-01479-y](https://doi.org/10.1038/s41386-022-01479-y); pmid: [36284231](https://pubmed.ncbi.nlm.nih.gov/36284231/)
71. J. R. Backstrom, M. S. Chang, H. Chu, C. M. Niswender, E. Sanders-Bush, Agonist-directed signaling of serotonin 5-HT_{2C} receptors. Differences between serotonin and lysergic acid diethylamide (LSD). *Neuropharmacology* **21** (Suppl.), 77S–81S (1999). doi: [10.1032492](https://doi.org/10.1032492)
72. G. Simic *et al.*, Does Alzheimer's disease begin in the brainstem? *Neuropathol. Appl. Neurobiol.* **35**, 532–554 (2009). doi: [10.1111/j.1365-2990.2009.01038.x](https://doi.org/10.1111/j.1365-2990.2009.01038.x); pmid: [19682326](https://pubmed.ncbi.nlm.nih.gov/19682326/)
73. H. Braak, E. Ghebremedhin, U. Rüb, H. Bratzke, K. Del Tredici, Stages in the development of Parkinson's disease-related pathology. *Cell Tissue Res.* **318**, 121–134 (2004). doi: [10.1007/s00441-004-0956-9](https://doi.org/10.1007/s00441-004-0956-9); pmid: [15338272](https://pubmed.ncbi.nlm.nih.gov/15338272/)
74. J. H. Lee, J. Ryan, C. Andreescu, H. Aizenstein, H. K. Lim, Brainstem morphological changes in Alzheimer's disease. *Neuroreport* **26**, 411–415 (2015). doi: [10.1097/WNR.0000000000000362](https://doi.org/10.1097/WNR.0000000000000362); pmid: [25830491](https://pubmed.ncbi.nlm.nih.gov/25830491/)

ACKNOWLEDGMENTS

We thank L. Acsády [HUN-REN Institute of Experimental Medicine (IEM), Hungary] for providing the macaque monkey brainstems; B. Hangya (HUN-REN IEM, Hungary) for help with AAV2/9-hSyn-DA4.4 virus; J. Huang (Duke University, USA) for help with the SOM-Cre mice; S. Arthaud (INSERM, Lyon, France) for help with vGluT2-Cre mice; A. L. Gundlach (University of Melbourne, Australia) for providing the anti-Relaxin-3 antibody; Sz. Takács for the help with the citrate buffer treatment; E. Misák for the help with the surgeries related to in vivo electrophysiological

experiments; and L. Kontra of the Bioinformatics Core Facility of HUN-REN IEM for the help with the genetic data analysis. We thank E. Sipos, the Virus Technology Unit of HUN-REN IEM, for technical support; P. Vági, the Microscopy Center at HUN-REN IEM for imaging technical support; K. Demeter and the Behavior Studies Unit of the HUN-REN IEM for behavioral experiment support; Z. Erdélyi, F. Erdélyi, and the staff of the Animal Facility and the Medical Gene Technology Unit of HUN-REN IEM for expert technical help with the breeding and genotyping of the mouse strains used in this study. We also thank S. Kőszegi and the Electron Microscopy Center at HUN-REN IEM for technical support. We also thank B. Török, P. Szocsics and Z. Maglóczy and the Human Brain Research Laboratory at HUN-REN IEM for their help with human tissues; Aphrodite Babakhani for her suggestions on the first draft of the manuscript; E. Szépné Simon and N. Kriczky for help with the experiments; and K. Iványi for other assistance. **Funding:** This work was funded by the following: Frontline Research Excellence Program of the Hungarian National Research, Development and Innovation Office, NRDI Fund 133837, Hungarian Brain Research Program, NAP2.0 2017-1.2.1-NKP-2017-00002 and NAP3.0 NAP2022-1/1/2022, European Union project RRF-2.3.1-21-2022-00004 within the framework of the Artificial Intelligence National Laboratory, and European Union project RRF-2.3.1-21-2022-00011 within the framework of the Translational Neuroscience National Laboratory (to G.N.); University of Zurich (to C.F.); European Research Council under the European Union's Horizon 2020 program, grant number 772452, nanoAXON (to J.S.); the National Academy of Scientist Education Program of the National Biomedical Foundation under the sponsorship of the Hungarian Ministry of Culture and Innovation, FEIF/646-4/2021-ITM_SZERZ (to R.Z.S., H.S., and G.N.); the New National Excellence Program of the Ministry of Innovation, Hungary, ÚNKP-23-3-I-SE-48 (to Á.O.); the New National Excellence Program of the Ministry of Innovation, Hungary, ÚNKP-23-2-II-SE-25 (to R.Z.S.); the New National Excellence Program of the Ministry of Innovation, Hungary, ÚNKP-22-3-II-SE-7 and ÚNKP-23-3-II-SE-24 (to K.Z.); Semmelweis 250+ Excellence PhD Fellowship, EFOP-3.6.3-VEKOP-16-2017-00009 (to K.Z.) Gedeon Richter Talentum Foundation in framework of Gedeon Richter Excellence PhD Scholarship of Gedeon Richter (to K.Z.). **Author contributions:** Conceptualization, K.Z., B.Z.B., J.B., V.T., A.M.B., and G.N.; Investigation, K.Z., R.Z.S., B.Z.B., and Á.O.; H.S. performed and analyzed anatomical experiments investigated by fluorescent microscopy, supervised by G.N.; V.T. performed and analyzed anatomical experiments investigated by electron microscopy, supervised by G.N.; K.Z. and R.Z.S. performed and analyzed the optogenetic behavioral experiments, supervised by G.N.; M.A. assisted in the

self-stimulation optogenetics experiment supervised by E.M.; B.Z.B. and K.Z. performed and analyzed the fiber photometry experiments, supervised by G.N.; A.M.B. performed and analyzed the in vivo electrophysiological experiments, supervised by G.N.; J.B. performed and analyzed the in vitro electrophysiological experiments, supervised by J.S.; C.S. performed and pre-analyzed the mRNA sequencing experiments, supervised by C.F.; K.Z. and B.Z.B. analyzed the RNA sequencing experiments, supervised by G.N.; K.Z. performed and analyzed the samples from rat, macaques, and humans, supervised by G.N. **Writing – Original Draft:** K.Z., R.Z.S., and G.N.; **Writing – Review & Editing:** all authors. **Competing interests:** Authors declare that they have no competing interests. **Data availability:** All relevant data are included in the manuscript and its supporting information files and table S, whereas all RNA sequencing data have been deposited in NCBI's Gene Expression Omnibus ([75](https://www.ncbi.nlm.nih.gov/geo/)) and are accessible through GEO Series accession number GSE264295 (<https://www.ncbi.nlm.nih.gov/geo/>). All viruses used in this study were obtained under specific material transfer agreements (MTA), as follows, AAVretro-hSyn-DIO-eGFP, AAVretro-EF1α-DIO-Chr2-mCherry, AAVretro-hSyn-S10-stGTACR2-FusionRed, AAVretro-hSyn-FLEX-jGCaMP8m, AAVretro-EF1α-FlpO-mCherry, AAVretro-EF1α-DIO-FlpO, AAV2/1-EF1α-DIO-mCherry were obtained from Addgene; AAVretro-EF1α-DIO-mCherry, AAV2/5-EF1α-DIO-eYFP, AAV2/2-EF1α-DIO-mCherry, AAV2/5-EF1α-DIO-hChr2(H134R)-eYFP, AAV2/5-EF1α-DIO-hChr2(H134R)-mCherry were obtained from UNC Vector Core; AAVretro1-EF1α-DIO-GCaMP6m was obtained from Braincase; AAV2/9-EF1α-DIO-Chr2-mCherry was obtained from Salk GT3 Vector Core; and AAV2/9-hSyn-FLEX-TVA-oG-nlsGFP-WPRE3, RabiesΔG-EnvA-mCherry were obtained from Charité Universitätsmedizin Berlin Viral Core Facility. **License information:** Copyright © 2025 the authors, some rights reserved; exclusive licensee American Association for the Advancement of Science. No claim to original US government works. <https://www.science.org/content/page/science-licenses-journal-article-reuse>

SUPPLEMENTARY MATERIALS

science.org/doi/10.1126/science.adr2191

Materials and Methods

Figs. S1 to S21

Tables S1 to S22

References ([75–90](#))

MDAR Reproducibility Checklist

Movie S1

Submitted 23 June 2024; accepted 21 November 2024
10.1126/science.adr2191